Chem

CellPress

Article

Expanding the toolbox of controlled/living branching radical polymerization through simulation-informed reaction design

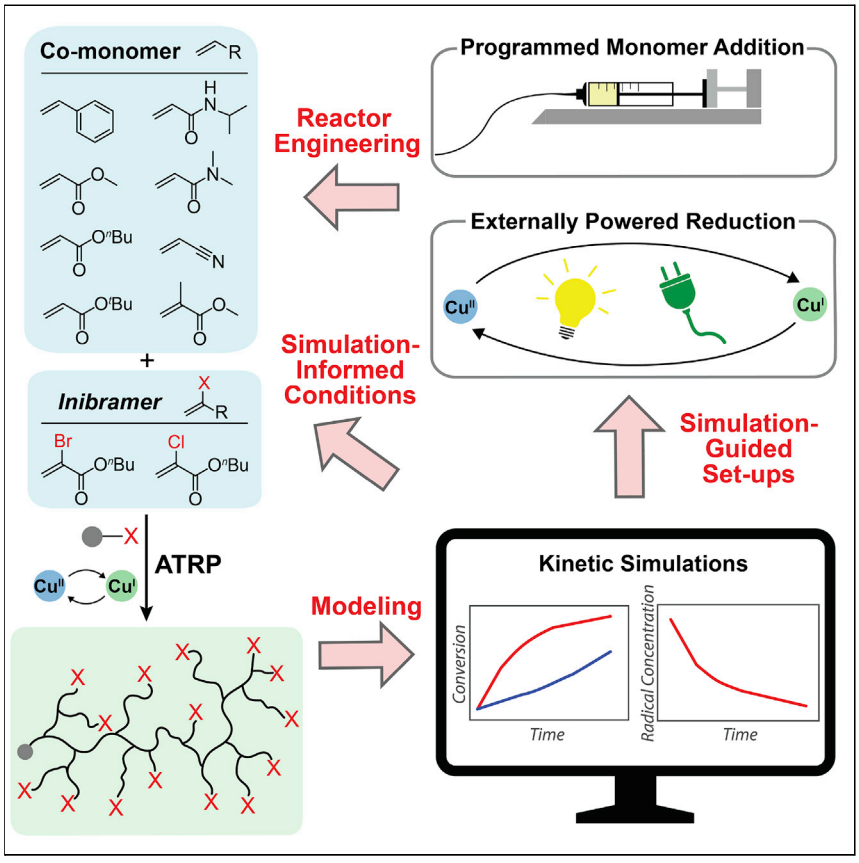

This work reports a site-specifically initiated chain-growth branching radical copolymerization. Mechanistic studies and kinetic simulations were carried out to guide the optimization of the reaction conditions. High monomer conversion and controlled degree of branching were achieved in the branching copolymerization of α-halogen acrylate with alkyl acrylates, styrene, acrylonitrile, and acrylamides.

Mengxue Cao, Yutong Liu, Xiaowei Zhang, Feng Li, Mingjiang Zhong

mingjiang.zhong@yale.edu

Highlights

A controlled/living branching polymerization was achieved

Mechanistic studies and kinetic simulations guided the reaction optimization

Branched polymers were synthesized from a broad range of vinyl monomers

Cao et al., Chem 8, 1–16
May 12, 2022
https://doi.org/10.1016/j.chempr.2022.02.022

Please cite this article in press as: Cao et al., Expanding the toolbox of controlled/living branching radical polymerization through simulation-informed reaction design, Chem (2022), https://doi.org/10.1016/j.chempr.2022.02.022

Chem

CellPress

Article

Expanding the toolbox of controlled/living branching radical polymerization through simulation-informed reaction design

Mengxue Cao,[1] Yutong Liu,[1,3] Xiaowei Zhang,[1] Feng Li,[1,4] and Mingjiang Zhong[1,2,5,*]

SUMMARY

Branched polymers with superior mechanical, photonic, and electrical properties have shown their growing advantages in biomedical applications, water treatment, and catalysis. Anchoring branched functional motifs onto select molecular-/nano-objects introduces structural hierarchy as well as combined and enhanced properties. To realize efficient grafting of branched functional polymers, a controlled chain-growth branching polymerization is desirable but remains underexplored. In this article, the chain-growth process was achieved by copolymerizing α-haloacrylate with conventional vinyl monomers via atom transfer radical polymerization. We conducted systematic mechanistic studies to obtain an optimal profile of the polymerization conditions, where an activator regeneration approach was employed. Assisted by kinetic simulations, a variety of vinyl monomers, including acrylates, styrene, acrylonitrile, and acrylamides, were successfully copolymerized with α-haloacrylate with high monomer conversion to produce well-defined branched polymers with tunable degrees of branching. The impact of controlled branching on the thermoresponsive properties was studied using the synthesized poly(*N*-isopropylacrylamide).

INTRODUCTION

Branched polymers, e.g., star-shaped,[1,2] bottlebrush-like,[3] randomly branched,[4–7] and dendritic polymers,[8–11] present unique properties, compared with their linear counterparts, such as high solubility, low intrinsic viscosity, and high end-group functionality.[12–14] Among these, dendrimers feature discrete molecular weights, uniformly distributed branching junctions, and precisely located end groups. Therefore, they exhibit enhanced performance in optoelectronics,[15–20] water treatment,[21] supramolecular chemistry,[22] and biomedical applications.[11,23,24] However, practical applications of dendrimers are impeded by their tedious and small-scale iterative synthesis and purification. As a desirable alternative, randomly (hyper)branched polymers can be synthesized via facile one-pot methods. Nevertheless, the performance of randomly branched polymers can be sacrificed by their ill-defined structures, resulting from the limited polymerization capabilities. Moreover, conventional branching polymerization strategies fail to efficiently install a branched or dendron-shaped polymer on a target molecular or nano-object, hindering the construction of higher-order architectures derived from dendritic building blocks.[25–29] Synthesizing uniformly branched polymers in a controlled and scalable manner remains a formidable challenge; however, there have been no breakthroughs until recent years.

The bigger picture

Dendritic polymers with advantageous physical properties have great potential in applications ranging from nanomedicine, bioimaging, to optoelectronic devices. Converting the fundamental studies of dendritic polymers to transformative research demands the development of a facile and scalable strategy to access dendritic polymers with preserved structural precision. Here, we developed a chain-growth branching polymerization that produces dendron-like well-defined branched polymers with diversely tunable functionalities. The polymerization can be conducted under industrially relevant conditions for free radical polymerization, and the reactivity can be regulated by clean and sustainable external power such as sunlight. We envision that this work will provide a versatile synthetic platform to promote the wide applications of dendritic functional polymers.

Please cite this article in press as: Cao et al., Expanding the toolbox of controlled/living branching radical polymerization through simulation-informed reaction design, Chem (2022), https://doi.org/10.1016/j.chempr.2022.02.022

Randomly branched polymers are typically synthesized through (1) polycondensation of AB_x or $A_x + B_y$ monomers ($x \geq 2$, $y \geq 3$), where the functional group A exclusively couples with the group B[30–32] or (2) self-condensing vinyl polymerization of monomers that are covalently linked with an initiating site.[33–38] Neither of these methods produces branched polymers with controlled molecular weight and low dispersity arising from the step-growth polymerization mechanism.

Controlled branching polymerizations were realized by introducing rationally designed monomers,[39–41] catalysts,[42–44] or reaction systems.[45–48] These developments enable a (pseudo-)chain-growth branching polymerization, where the continuous generation of new branched chains can be suppressed throughout the entire polymerization. Among those developed strategies, the controlled/living radical polymerization (CRP)[49,50] involving a polymerization-induced branching process emerged as a versatile method that can potentially be applied for a wide range of monomers and conducted in various reaction media.[25,51–56] In this method, a vinyl monomer containing an α-functional group was synthesized for the copolymerization with conventional vinyl monomers that are used in a free radical polymerization.[55,56] The α-functionality in the new monomer serves as an initiating site only after the monomer is integrated into the polymer chain, thereby creating a branching junction in the same chain. The term of *inibramer* was used to capture the triple role of the designed monomer—*ini*tiator, *bra*nching junction creator, and mono*mer*. The seminal work by Yamago and coworkers employed vinyl tellurides as *inibramer*s in telluride-mediated CRP to synthesize branched polyacrylates and polystyrene[51] with a dispersity index (*Đ*) in the range of 1.40–3.25.[55] We recently reported the controlled synthesis of branched polystyrene and polyacrylates through atom transfer radical polymerization (ATRP) involving an *n*-butyl α-bromoacrylate (BBA) *inibramer*.[25] Different from the telluride-mediated CRP, Cu^I-catalyzed alkyl halide activation process generated the propagating radical in ATRP without requiring the addition of extra free radical initiators (FRIs). Hence, branched polymers with a relatively low *Đ*, down to 1.20, were obtained with different degrees of branching (DBs). Moreover, this FRI-free system allowed for the development of a site-specifically initiated branching polymerization. Aided by the facile installation of ATRP initiators to different substrates, diverse well-defined hierarchically branched polymers were covalently assembled from dendron-like molecular building blocks.[25]

Despite the preliminary success, further application of the BBA-enabled branching polymerization was limited by its low monomer conversion. For instance, the branching copolymerization of *n*-butyl acrylate (*n*BA) and BBA usually stopped at an *n*BA conversion below 25%. Furthermore, it was difficult to extend the system to monomers with reactivities different from styrene and acrylates due to the complex polymerization system that simultaneously involves more than twenty elementary reaction processes and a variety of reaction condition parameters (Scheme 1). In this work, detailed mechanistic studies of the BBA-enabled branching polymerization were carried out by combining a series of experimental and computational techniques. Knowledges attained from the studies with quantitatively evaluated elementary steps were integrated into kinetic modeling to guide the further development. The simulation-informed experimental design led to significantly enhanced monomer conversion (>50% *inibramer* conversion) and successfully expanded the scope of monomers to cover a nearly complete library of monomers that can be polymerized under ATRP conditions.

[1]Department of Chemical and Environmental Engineering, Yale University, New Haven, CT 06511, USA

[2]Department of Chemistry, Yale University, New Haven, CT 06511, USA

[3]College of Chemistry, Nankai University, Tianjin 300071, People's Republic of China

[4]Present address: WPI Nano Life Science Institute, Kanazawa University, Kakuma-machi, Kanazawa 920-1192, Japan

[5]Lead contact

*Correspondence: mingjiang.zhong@yale.edu

https://doi.org/10.1016/j.chempr.2022.02.022

Please cite this article in press as: Cao et al., Expanding the toolbox of controlled/living branching radical polymerization through simulation-informed reaction design, Chem (2022), https://doi.org/10.1016/j.chempr.2022.02.022

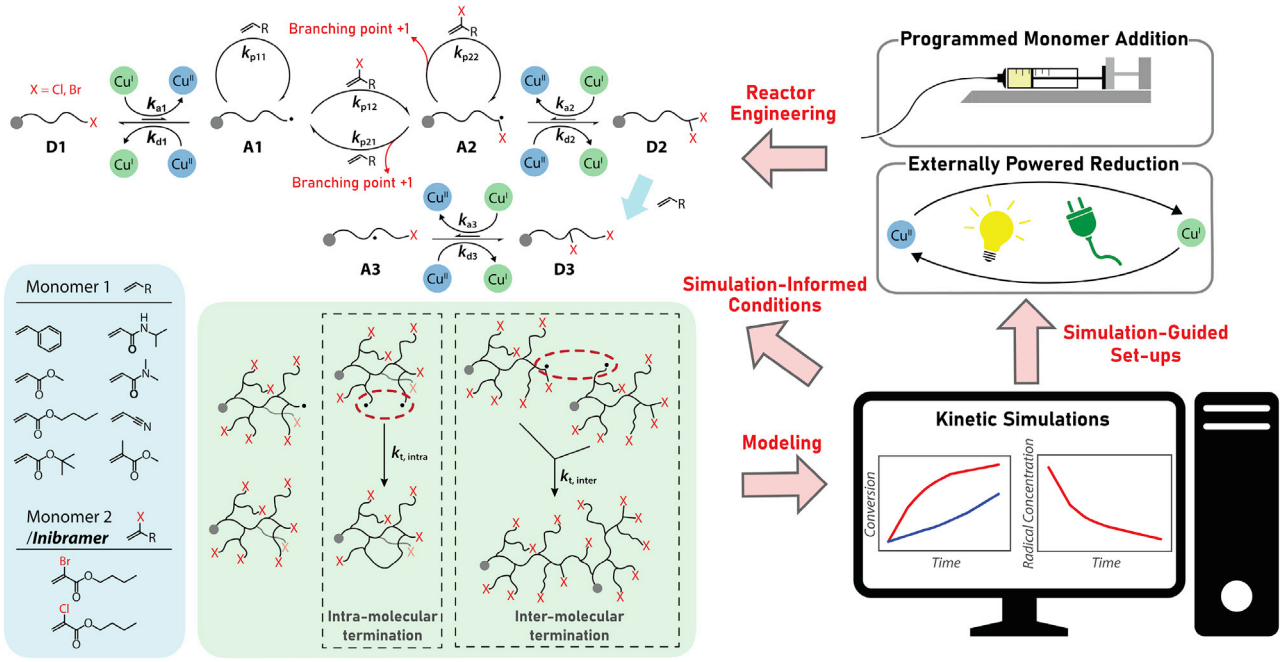

Scheme 1. Mechanistic studies of atom transfer radical branching copolymerization of *inibramer*s and conventional vinyl monomers

Monomers including *n*-butyl acrylate, methyl acrylate, and styrene were reported in our previous work.[25]

RESULTS AND DISCUSSION

Mechanistic studies and kinetic simulations

Scheme 1 presents the proposed mechanism of the *inibramer*-enabled branching polymerization, detailed with elementary reaction steps. Although our previous experimental data were consistent with the proposed mechanism, validating and kinetically quantifying each elementary step became keys to addressing the remaining challenges. This comprehensive knowledge about such a complex polymerization system also allowed us to carry out kinetic simulations to efficiently discover the optimal conditions for various monomers.

The controlled polymerization and livingness in ATRP are ensured by a reaction equilibrium established between the propagating radical formation and deactivation processes.[57–61] Specifically, the metal ligand (L) complex in the lower oxidation state, e.g., Cu^{I}/L, activates an alkyl halide (R–X, X = Br or Cl) to generate a propagating radical (R•), and Cu^{II}X/L. Cu^{II}X/L can reversibly deactivate R• to reform the dormant species R–X. In a BBA-participating ATRP, multiple ATRP equilibria are present and compete with one another. In addition to the regular ATRP initiators and polymers end-functionalized with halogen (Scheme 1, **D1**), R–X derived from BBA (Scheme 1, **D2** and **D3**) significantly altered the polymerization kinetics. Although the C–Br bond of BBA with a bond dissociation energy (BDE) of 80.7 kcal/mol[25] is sufficiently high to stay intact in the presence of Cu^{I}/L, the radical addition of BBA produced a new radical center (Scheme 1, **A2**) tethered with a Br atom at the α-position. We previously hypothesized that **A2** can be deactivated by Cu^{II}Br/L to form a *gem*-dibromo dormant species (**D2**), but we lacked direct experimental evidence. Herein, we conducted FRI-initiated homopolymerizations of BBA to confirm the occurrence of the deactivation of **A2** and the formation of **D2**. During the homopolymerizations of BBA, Cu^{II}Br/bpy was added in excess to the reaction for nuclear magnetic resonance (NMR) spectroscopy studies (see supplemental information).

The signal at the chemical shift of 55.36 ppm observed in the ^{13}C NMR spectrum suggested the formation of *gem*-dibromo chain ends (Figure S1).

Ethyl 2,2-dibromopropanoate (EDBP) was used as a model compound to study the mechanism and kinetics of junction formation from an alkyl dibromide center **D2**. The reaction of EDBP and Cu^{I}/L was carried out in the presence of (2,2,6,6-tetramethylpiperidin-1-yl)oxyl (TEMPO). Adding the TEMPO radical trap decreased the abundance of the biradical termination products (Scheme S4; Figure S2), confirming the formation of free radicals from Cu^{I}/L activation. A carbene intermediate derived from **D2** was not detected when a carbene trap 2,3-dimethyl-2-butene or benzyl alcohol was employed (see supplemental information).

The rate coefficient of the first C–Br activation of EDBP (k_{a2}), the rate coefficient of the corresponding deactivation (k_{d2}), and the ATRP equilibrium constant (K_{ATRP}) were then estimated to be 83.4 M^{-1} s^{-1}, 9.5 × 10^{7} M^{-1} s^{-1}, and 8.8 × 10^{-7}, respectively (see supplemental information), when using *N*,*N*,*N*′,*N*″,*N*″-pentamethyldiethylenetriamine (PMDETA) as a ligand and acetonitrile (MeCN) as a solvent at 60°C. The bromo-containing radical **A2** can, in addition to being deactivated by Cu^{II}Br/L, add to either an *n*BA or a BBA monomer to form a **D3** radical with a new activatable tertiary R–X site at the penultimate position from the polymer chain end. The corresponding activation (k_{a3}) and deactivation (k_{d3}) rate coefficients of this resultant tertiary R–X were approximated to be the same as those for ethyl α-bromoisobutyrate (EBiB) in the subsequent kinetic simulations.

EDBP was used to initiate ATRP of *n*BA to investigate the formation of a branching junction (Scheme S5). Absence of the monobromo-substituted tertiary carbon and presence of the quaternary carbon originating from EDBP in a ^{13}C NMR spectrum of the resultant polymers (Figure S40) confirmed the postulated double-initiation of the alkyl *gem*-dibromide species. A significantly slower polymerization, compared with an ATRP initiated by a regular initiator, i.e., ethyl 2-bromopropanoate (EBP) or EBiB, was observed in EDBP-initiated ATRP with the same concentration of C–Br initiating sites (Figure S3). This could be attributed to an accelerated intramolecular biradical termination process in the polymer chains containing more than one radical center. This hypothesis was partially confirmed by the fact that nearly the same polymerization kinetics was observed in ATRP using ethylene bis(2-bromoisobutyrate) (EBBiB), i.e., a bifunctional initiator with similar structure to EBiB. We evaluated the rate of the intrachain termination by numerically fitting the polymerization kinetics resulting from EBBiB initiation (see supplemental information). The rate of intrachain termination was found to be 4 orders of magnitude higher than that of diffusion-limited interchain termination.[62,63] This result supported our hypothesis that an exacerbated radical termination could be the main cause of the low conversion in the branching copolymerization.

A complete list of rate coefficients employed in the kinetic simulations is available in Table S2. The copolymerization of *n*BA and BBA via a conventional ATRP was simulated (Figure 1A). An initial molar ratio of 300/30 was employed for *n*BA/BBA with respect to the EBP initiator. Other side reactions or factors were not taken into account for simplicity, including chain-length-dependent radical termination,[64,65] Cu^{I}-catalyzed radical termination,[66–69] and disproportionation of Cu^{I}/L.[70] Consistent with the experimental observation, stoichiometrically unbalanced consumption of *n*BA and BBA was obtained in a one-pot copolymerization due to the highly polarized polymerization reactivity (r_{BBA} = 9.77, r_{nBA} = 0.24).[71] This gradient copolymerization produced branched copolymers rich in BBA at the early stage of the

Please cite this article in press as: Cao et al., Expanding the toolbox of controlled/living branching radical polymerization through simulation-informed reaction design, Chem (2022), https://doi.org/10.1016/j.chempr.2022.02.022

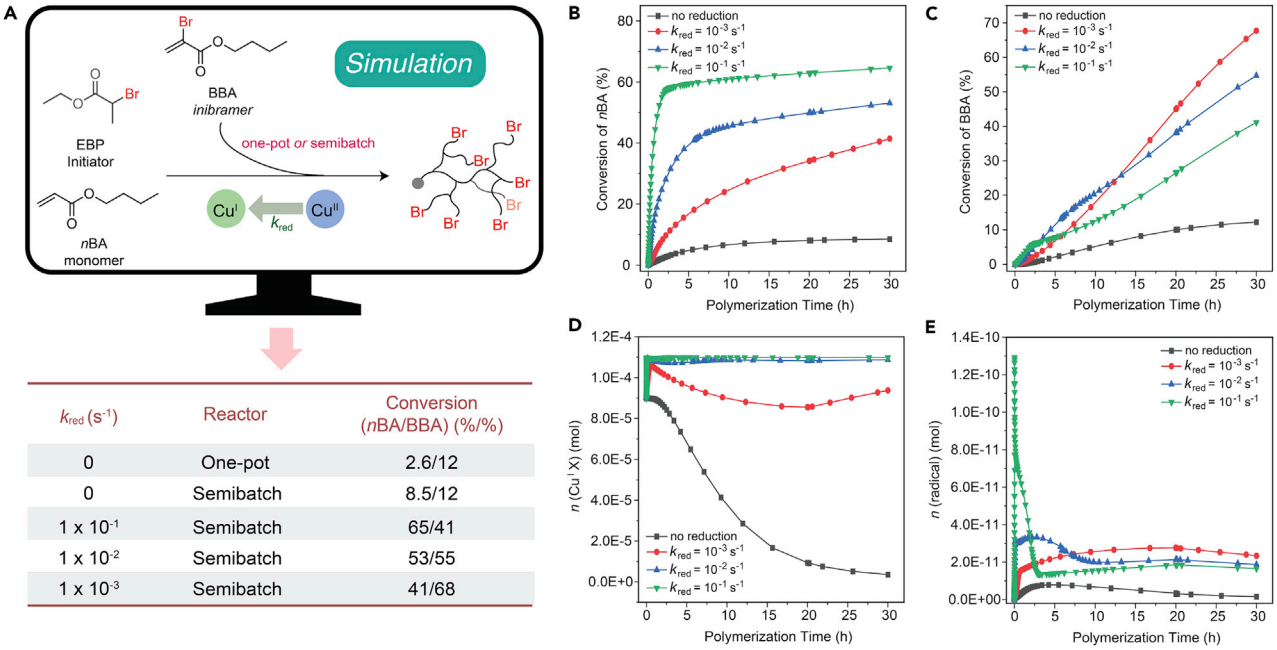

k_{red} (s^{-1})	Reactor	Conversion (*n*BA/BBA) (%/%)
0	One-pot	2.6/12
0	Semibatch	8.5/12
1 x 10^{-1}	Semibatch	65/41
1 x 10^{-2}	Semibatch	53/55
1 x 10^{-3}	Semibatch	41/68

Figure 1. Kinetic simulations for copolymerizations of *n*BA and BBA via activator regeneration ATRP

(A) Simulated reaction conditions and simulation results. $[nBA]_0/[BBA]_{total}/[EBP]_0/[CuBr]_0/[CuBr_2]_0$ = 300/30/1/0.9/0.2, with PMDETA as ligand and MeCN as solvent at 60°C for 30 h. $[nBA]_0$ = 4.75 M. For semibatch reactions, BBA was slowly added over 20 h at the rate of 1.5 equiv/h as a solution with [BBA] = 2.0 M from the beginning.

(B) *n*BA conversion versus polymerization time.

(C) BBA conversion versus polymerization time.

(D) Activator amount versus polymerization time.

(E) Radical amount versus polymerization time.

(B–E) Results from simulations based on semibatch reactions.

polymerization and an ill-defined distribution of branching junctions across the branched chain. After the conversion of *n*BA reached 2.5%, the amount of Cu^I/L activator sharply decayed from the initial 0.090mmol to 0.002 mmol, resulting in a slowdown in the polymerization (Figure S6). The rapid decrease in the activator concentration compared with a normal ATRP of *n*BA was ascribed to the accelerated radical termination, which irreversibly generated Cu^{II}Br/L deactivator from Cu^I/L, when more propagating radicals were introduced as result of the BBA incorporation. Each added BBA provided an additional C–Br bond that can be activated by Cu^I/L, and the irreversible consumption was further enhanced in a branching polymerization accompanied with fast intrachain termination. Thus, chain propagation that favored BBA incorporation over *n*BA in the one-pot copolymerization led to the challenges in achieving well-defined polymer structure and polymerization livingness.

A semibatch copolymerization strategy was integrated into the simulation model, where the BBA monomer with a higher activity was slowly fed into the polymerization at a rate of 1.5 equiv/h (Figure 1A). The slightly improved regulation of cross-propagation behaviors provided higher monomer conversion, but the polymerization stopped at around 8% conversion of *n*BA due to the increased radical termination (Figure 1B, black curve). The relatively low degree of BBA incorporation limited the tunability of DB (Figure 1C, black curve).

To address the challenges in the branching polymerization inherently associated with the uncontrolled radical concentration, a reducing power that can continuously

Please cite this article in press as: Cao et al., Expanding the toolbox of controlled/living branching radical polymerization through simulation-informed reaction design, Chem (2022), https://doi.org/10.1016/j.chempr.2022.02.022

regenerate Cu^{I}/L from Cu^{II}X/L was applied in the kinetic modeling to precisely modulate the Cu^{II}/Cu^{I} ratio and the radical concentration. With a pseudofirst order reduction rate coefficient (k_{red}) of 1×10^{-1} s^{-1},[72] the polymerization of *n*BA stopped after 2.5 h at a conversion of *ca*. 60% (Figure 1B, green curve). Although the incorporation of BBA continued after the *n*BA conversion profile plateaued, the propagation rate decreased, and the polymerization ended with a relatively low BBA conversion of 41% (Figure 1C, green curve). Although a high activator concentration was maintained (Figure 1D, green curve), an excess number of radicals led to the formation of terminated chains 2–3 orders of magnitude more than that without reducing power at the very early stage. The radical concentration then dropped rapidly even under a high activator concentration due to the loss of living chain ends (Figure 1E, green curve). When the Cu^{II}X/L reduction became 10 times slower, despite the decrease in the polymerization rate of *n*BA at the early stage, a more sustainable polymerization was achieved with an *n*BA conversion of 45% after 8 h (Figure 1B, blue curve). The conversion of BBA also increased (Figure 1C, blue curve). No conversion plateau of *n*BA was observed (Figure 1D, red curve), and the conversion of BBA was significantly increased (Figure 1C, red curve) when a reduction rate was decreased further by an order of magnitude. The well-regulated activator concentration allowed the maintenance of a relatively high radical concentration, sustaining the copolymerization with a high chain end fidelity (Figures 1D and 1E, red curves).

The simulation results informed us that the activator regeneration process with a moderate reduction rate was critical for a branching copolymerization with high monomer conversion. The activator regeneration process maintains a sufficient amount of activators for the polymerization; the regulated low activator concentration suppressed the radical terminations. The optimal reduction rate according to simulation results matched the experimental values in activator regeneration ATRPs.[73] Therefore, activator regeneration ATRP was considered an ideal solution to improve the control and livingness of the BBA-enabled branching copolymerization.

Copolymerization of (meth)acrylates and BBA via photoredox-mediated ATRP (photo-ATRP)

Although various types of reducing power, e.g., light,[74–79] cathodic current,[80–82] *in situ* generated free radicals,[83,84] ascorbic acid,[85] tin(II) 2-ethylhexanoate,[86] zero-valent metal,[87] and mechanical forces[88] have been introduced to the activator regeneration ATRP, the simulation results suggested that reduction reactions with a precisely controlled and tunable rate were needed to sustain the branching copolymerization with minimal radical termination. We first copolymerized *n*BA and BBA under electrochemical ATRP conditions. Digitally controlled number of the transferred electrons and the cathodic current were envisioned to be quantitatively correlated with the amount of reduced Cu^{II}X/L and the reduction rate, respectively.[80,81] However, the mass-transfer limitation of the regenerated activator in such a heterogeneous system severely impeded the electroreduction (see supplemental information).

Photo-ATRP, where light stimulates the ligand to reduce Cu^{II}X/L to Cu^{I}/L in a homogeneous system, was then investigated under the irradiation of a 385–400 nm LED strip light source (Table 1, entry 1–9).[74,75] With the presence of 100 ppm Cu species relative to *n*BA, addition of 8 equiv of BBA with respect to the initiator at a rate of 0.8 equiv/h led to the formation of branched poly(*n*-butyl acrylate) (P*n*BA) with $M_{n,theo}$ of 21.0 kDa and $M_{n,GPC}$ of 10.1 kDa (Table 1, entry 1), where $M_{n,theo}$ and $M_{n,GPC}$ stand for the number-average molecular weights that were theoretically

Please cite this article in press as: Cao et al., Expanding the toolbox of controlled/living branching radical polymerization through simulation-informed reaction design, Chem (2022), https://doi.org/10.1016/j.chempr.2022.02.022

Table 1. Copolymerization of BBA with different monomers via photo-ATRP[a]

Entry	M	[M]/[BBA]/[I]	Cu loading[b] (ppm)	Time (h)	Feed rate[c] (equiv/h)	Conversion (M/BBA) (%/%)	$M_{n,theo}$ (kDa)	$M_{n,GPC}$ (kDa)	$M_{n,MALLS}$ (kDa)	$Đ$	S_n[d]
1	*n*BA	300/8/1	100	24	0.8	50/98	21.0	9.3	19.0	1.51	9.1
2	*n*BA	300/16/1	100	31	0.8	41/85	18.8	8.7	16.5	1.62	4.4
3	*n*BA	300/16/1	100	45	0.4	49/61	20.9	10.1	24.0	1.27	7.6
4	*n*BA	300/16/1	175	45	0.4	40/81	18.0	8.5	17.2	1.42	4.4
5	*n*BA	300/16/1	250	45	0.4	32/62	14.4	6.9	12.9	1.28	4.6
6	*n*BA	600/32/1	100	31	1.6	37/88	34.2	9.8	27.6	1.94	3.9
7	*n*BA	600/32/1	175	31	1.6	26/72	24.4	6.5	22.5	1.41	3.2
8	*n*BA	300/7.2/1	100	48	–[e]	93/100	37.3	14.5	37.1	1.81	18.2
9	*n*BA	300/3.6/1	100	36	–[e]	94/100	36.7	20.9	33.1	1.66	34.3
10	*t*BA	300/16/1	100	31	0.8	35/66	15.7	7.8	12.2	1.48	4.7
11	MMA	300/7/1	100	24	–[e]	46/94	15.5	2.8	–	1.54	9.8
12	AN	300/8/1	100	24	–[e]	23/81	5.3	4.5	18.8	1.77	5.0
13	AN	300/8/1	100	24	0.8	39/75	7.8	6.9	15.7	1.65	9.1
14	AN	300/8/1	100	31	0.4	61/61	11.0	11.9	23.9	1.40	17.0

[a]Conditions for *n*BA: $[EBiB]_0/[CuBr_2]_0/[Me_6TREN]_0$ = 1/0.03/0.18 for 100 ppm Cu loading (Me_6TREN = tris[2-(dimethylamino)ethyl]amine). For higher Cu loading, only change $[CuBr_2]_0$. $[nBA]_0$ = 4.7 M in *N*,*N*-dimethylformamide (DMF) at room temperature in a photoreactor with wavelength of 385–400 nm. Conditions for *t*BA: same as *n*BA but with $[tBA]_0$ = 4.6 M. Conditions for MMA: $[EBPA]_0/[CuBr_2]_0/[TPMA]_0$ = 1/0.03/0.18 (TPMA, tris(2-pyridylmethyl)amine). $[MMA]_0$ = 4.2 M in DMF. Conditions for AN: $[EBPA]_0/[CuBr_2]_0/[Me_6TREN]_0$ = 1/0.03/0.18. $[AN]_0$ = 7.2 M in dimethyl sulfoxide (DMSO).

[b]Cu loading is with respect to the monomer amount. Cu species were completely dissolved under all polymerization conditions to rule out the heterogeneous reactions.[89]

[c]Slow feeding started after 1 h of polymerization.

[d]$S_n = DP_M/(1 + 2DP_{BBA})$, degree of polymerization (DP).

[e]One-pot copolymerization.

predicted based on the monomer conversion and evaluated by gel permeation chromatography (GPC), respectively. The evident discrepancy between $M_{n,theo}$ and $M_{n,GPC}$ suggested a branched architecture with a smaller hydrodynamic volume compared with its linear counterpart. The conversions of *n*BA and BBA were 50% and 98%, respectively, far exceeding those obtained under conventional ATRP conditions.[25] Under conventional ATRP conditions, the slowdown of propagation along with BBA incorporation resulted in limited conversions of both comonomers (e.g., <20% of *n*BA and <50% of BBA). On the contrary, by utilizing photo-ATRP, the propagation of both *n*BA and BBA was maintained at a nearly constant rate (Figure 2A), suggesting the uniformly distributed branching junctions. A relatively low dispersity ($Đ$ = 1.51) was obtained with Cu loading as low as 100 ppm. The DB was evaluated by a spacing value S_n that equals the average number of monomers inserted between two neighboring branching junctions. S_n can be calculated based on the conversion of *n*BA and BBA, as every polymerized BBA is able to create a branching junction and *n*BA does not contribute to the branching. By increasing the feed amount of BBA from 8 to 16 equiv, S_n decreased from 9.1 to 4.4, although a lower conversion and a higher $Đ$ were observed (Table 1, entry 2).

To seek the optimal conditions, a lower feed rate of BBA (0.4 equiv/h) was employed, generating branched P*n*BA with $Đ$ as low as 1.27 but also a lower DB (S_n = 7.6) (Table 1, entry 3). If a higher Cu loading (175 ppm) and a lower feed rate (0.4 equiv/h) were introduced simultaneously, $Đ$ decreased from 1.62 to 1.42 with unchanged conversion and DB (S_n = 7.6) (Table 1, entry 4). A higher initial $Cu^{II}X/L$ concentration with the same ligand concentration and light intensity rendered a higher ratio of Cu^{II}/Cu^{I}, resulting in a decelerated polymerization with lower $Đ$. Since the incorporation of BBA led to an increase in the radical concentration, $Đ$ increased over the course of copolymerization. With a lower feed rate of BBA, the additional radical centers derived from the branching junctions were able to grow in a more

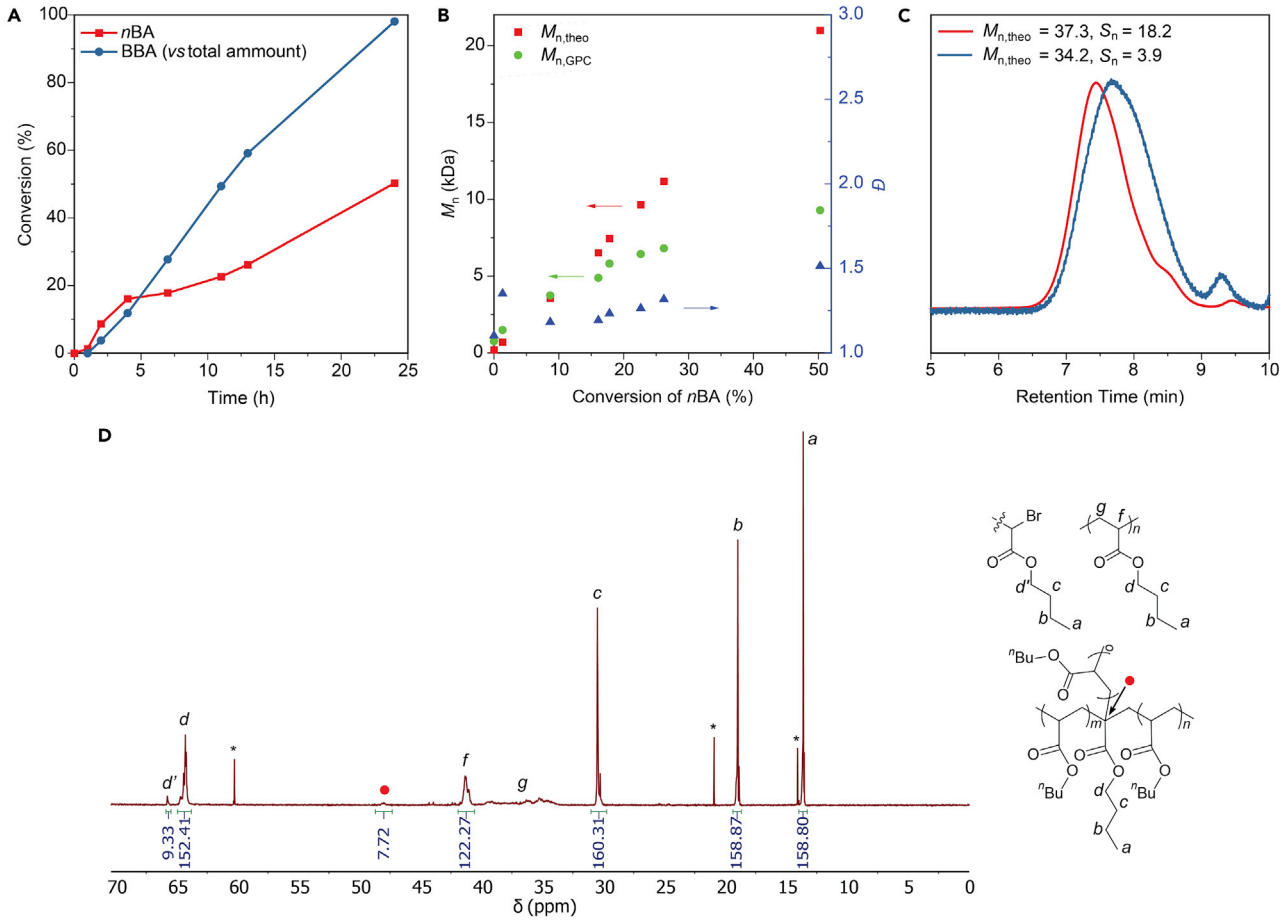

Figure 2. Copolymerization of *n*BA and BBA via photo-ATRP

(A and B) $[n\text{BA}]_0/[\text{BBA}]_{total}/[\text{EBiB}]_0/[\text{CuBr}_2]_0/[\text{Me}_6\text{TREN}]_0$ = 300/8/1/0.03/0.18; BBA was slowly fed at a rate of 0.8 equiv/h: (A) monomer conversion calculated from ^{1}H NMR analysis versus polymerization time; (B) M_n and $Đ$ versus *n*BA conversion.

(C) GPC traces of branched P*n*BAs with similar $M_{n,theo}$ but varied DB (represented by S_n) (Table 1, entries 6 and 8).

(D) Quantitative ^{13}C NMR spectrum of the branched P*n*BA (Table 1, entry 1) in $CDCl_3$ (residual ethyl acetate marked by asterisks).

controlled manner due to the decreased kinetic chain length. The propagation rate also increased at a lower addition rate of BBA due to the decelerated termination. Further increasing the Cu loading to 250 ppm generated polymers with $Đ$ as low as 1.28 but a much lower M_n (Table 1, entry 5). Branched P*n*BA with both high M_n and DB was synthesized by employing higher ratios of both *n*BA and BBA with respect to the initiator (Table 1, entry 6–7). Although monomer conversion decreased due to a high feed rate of BBA (1.6 equiv/h), $M_{n,theo}$ of the final branched P*n*BA exceeded all previous results and reached 34.2 kDa. The low $M_{n,GPC}$ of 9.8 kDa indicated its high DB (S_n = 3.9) despite a relatively high $Đ$ of 1.94 (Table 1, entry 6). Increasing the Cu concentration from 100 to 175 ppm generated branched P*n*BA with a lower $Đ$ of 1.41 (Table 1, entry 7).

According to the prediction from kinetic simulations, the reduction rate in photo-ATRP was moderate enough to maintain a reasonable level of radical concentration even in a one-pot copolymerization of *n*BA and BBA. The one-pot copolymerization was experimentally investigated with a 100 ppm Cu loading to suppress the radical termination. At different molar ratios of *n*BA to BBA, polymers with varied DBs were accessed at nearly quantitative conversions of both monomers after 48 h (Table 1,

Please cite this article in press as: Cao et al., Expanding the toolbox of controlled/living branching radical polymerization through simulation-informed reaction design, Chem (2022), https://doi.org/10.1016/j.chempr.2022.02.022

entry 8–9). The consumption rates of the two monomers in the one-pot photo-ATRP were consistent with their reactivity ratios, where BBA was converted much faster at the beginning of the copolymerization (Figure S17A). According to the kinetic data, a gradient copolymer—specifically, a star-like P*n*BA with a branched core—was synthesized through the one-pot method. The GPC traces, however, indicated the low initiation efficiency and the occurrence of radical coupling (Figure S17C). As expected, the higher feed ratio of BBA generated branched P*n*BA with a higher DB but a higher *Đ*. The broadened tuning range of DB opened a way to synthesizing polymers with similar molecular weight but different S_n values (Figure 2C). Branched P*n*BA with a lower S_n, i.e., higher DB, exhibited a much smaller hydrodynamic volume or $M_{n,GPC}$ due to the more globule-shaped structure.

The structure of a branched P*n*BA in Table 1, entry 1, was investigated by the quantitative ^{13}C NMR spectroscopy (Figure 2D). The integrals of the chemical shifts corresponding to C of the *n*-butyl groups on the main chain (152 C_d) and adjacent to the chain end (9 C_d′) were consistent with the theoretical values calculated from the monomer conversion, i.e., 150 nonterminal repeating units and 9 units near active chain ends per polymer chain. The chemical shift of C near the bromine chain end also verified the high chain fidelity of our branched polymers. It is noteworthy that the previously observed back-biting reactions[51] may take place with minimal impact on the overall DB and chain end fidelity.

In addition to the previously demonstrated semibatch strategy, tuning the reactivity ratio of the comonomer and BBA is an alternative way to achieve a uniform distribution of branching junctions in the one-pot synthesis. One-pot copolymerization of methyl methacrylate (MMA) and BBA (r_{MBA} = 0.16, r_{MMA} = 0.19, methyl α-bromoacrylate [MBA], as an analogy of BBA)[90] provided a nongradient copolymerization kinetics (Table 1, entry 11; Figure S20A). Unfortunately, low molecular weight fractions appeared in the GPC traces (Figure S20C), corresponding to side products originating from the β-scissions of polymer chains containing a tertiary backbone radical.[53] Chen and coworkers recently reported that branching copolymerization of fluorinated methacrylates with a 2-bromotrifluoropropene *inibramer* yielded polymers without detectable β-scission products.[54] Therefore, designing new *inibramer*s with rationally tuned electronic structures and reactivity could be one of the future research directions to enhance the versatility of the branching polymerizations.

In our previous work, we have demonstrated that BBA can be applied to synthesize branched poly(*tert*-butyl acrylate) (P*t*BA) (Table 1, entry 10), poly(methyl acrylate), and polystyrene.[25] Next, taking advantage of the activator regeneration ATRP, we expanded the monomer scope ranging from high-to-low activity monomers in ATRP, including acrylonitrile (AN) and acrylamides.

Copolymerization of acrylonitrile (AN) and BBA via photo-ATRP

The AN monomer with a K_{ATRP} 2–3 orders of magnitude higher than *n*BA requires more carefully regulated radical generation rate for a controlled branching polymerization.[91–93] Our initial model studies on the homopolymerization of AN under a photo-ATRP environment suggested that a highly active initiator ethyl α-bromophenylacetate (EBPA) was needed to realize reasonably high initiation efficiency, even when the high activity ligand Me_6TREN was used. The homopolymerization of AN proceeded in a well-controlled manner with 100 ppm of Cu species. The copolymerization of AN and BBA was then conducted by both one-pot and semibatch methods (Table 1, entry 12–14). The copolymerization with slow addition of BBA

Please cite this article in press as: Cao et al., Expanding the toolbox of controlled/living branching radical polymerization through simulation-informed reaction design, Chem (2022), https://doi.org/10.1016/j.chempr.2022.02.022

Table 2. Copolymerization of BCA and acrylamides via Cu^0-mediated ATRP[a]

Entry	M	[M]/[BCA]/[I]	Time (h)	Feed rate[b] (equiv/h)	Conversion (M/BCA) (%/%)	$M_{n,theo}$ (kDa)	$M_{n,GPC}$ (kDa)	$M_{n,MALLS}$ (kDa)	$Đ$	S_n
1	DMAA	500/0/1[c]	28	–	29/–	14.4	25.5	–	2.49	–
2	DMAA	500/4/1	34	0.4	21/93	11.0	4.0	9.8	2.04	12.4
3	DMAA	500/4/1	34	0.2	18/74	9.4	3.5	10.3	1.94	13.0
4	DMAA	500/8/1	34	0.4	14/65	7.7	1.4	19.1	2.75	6.1
5	NIPAM	500/4/1	34	0.2	23/72	13.6	6.1	11.0	1.82	17.0

[a]Conditions for DMAA: $[MeClPr]_0/[CuCl_2]_0/[Me_6TREN]_0$ = 1/0.75/1.5. Cu wire l = 0.3 cm, d = 1 mm. $[DMAA]_0$ = 6.8 M in DMSO at room temperature. Conditions for NIPAM: same as DMAA but with $[NIPAM]_0$ = 6.1 M.
[b]Slow feeding of BCA started after 2 h of polymerization.
[c]Homopolymerization of DMAA.

outperformed the one-pot copolymerization in terms of monomer conversion as well as polymer dispersity, due to the different reactivities between AN and BBA (r_{MBA} = 4.20, r_{AN} = 0.08, MBA as an analogy of BBA).[94]

The conversion of AN in a one-pot copolymerization was much lower than that of the BBA comonomer, although the propagation of both monomers was observed throughout the course of the polymerization (Figure S21A). The branched polyacrylonitrile (PAN) synthesized from the one-pot method had a $M_{n,MALLS}$ of 18.8 kDa with a $Đ$ of 1.77 (Table 1, entry 12). The inconsistency between $M_{n,MALLS}$ and $M_{n,theo}$ was presumably due to the relatively low initiation efficiency and the coupling terminations. The significantly lower $M_{n,GPC}$ of 4.5 kDa compared with $M_{n,MALLS}$, however, proved the branching process. Slow feeding of BBA suppressed the termination reactions, thus providing a higher conversion of AN and a smaller difference between $M_{n,MALLS}$ and $M_{n,theo}$ (Table 1, entry 13–14). The copolymerization with a lower BBA feed rate generated branched PAN with a higher M_n and a lower $Đ$. When BBA was added at a rate of 0.4 equiv/h, continuous consumption of both AN and BBA was observed, producing branched PAN with $M_{n,theo}$ of 11.0 kDa and $Đ$ of 1.40 (Table 1, entry 14; Figure S23A). The ^{1}H NMR spectrum of branched PAN showed good agreement with the theoretical values (Figure S41). The integrals of chemical shifts *e* and *f* corresponding to the AN units and *h*–*j* corresponding to the BBA units were consistent with the conversion of the two comonomers. Overall, the conversion of AN in the copolymerization was slightly limited compared with that of *n*BA in the *n*BA/BBA copolymerization because of the different reactivity ratios in the two systems and the higher K_{ATRP} of AN. However, by employing a slower feed rate of BBA, branched PAN with $Đ$ as low as 1.40 could be synthesized.

Copolymerization of acrylamides with *inibramer* via ATRP in the presence of Cu^0

ATRP of acrylamides with high livingness remains a challenge due to the polymer complexation to the catalyst, nucleophilic reactions toward the C–X (X = Br, Cl) chain end, as well as low K_{ATRP}.[95–97] The conventional ATRP of acrylamides exhibited low monomer conversion and high dispersity. The aforementioned difficulties in branching polymerization can be amplified when acrylamides are copolymerized with *inibramer*s. Current progress in achieving ATRP of acrylamides primarily relies on the systems in the presence of Cu^0 in a polar medium where catalyst and polymer interaction is limited and K_{ATRP} is increased.[98] We first conducted the homopolymerization of *N*,*N*-dimethylacrylamide (DMAA) in DMSO using a Cu wire as the supplemental activator and reducing agent. By utilizing methyl 2-chloropropionate (MeClPr) as the initiator and $CuCl_2$/Me_6TREN as the deactivator, we observed a continuous increase in the monomer conversion (Figure S24A), yet a relatively high dispersity ($Đ \sim 2$) (Table 2, entry 1). $CuCl_2$ was employed here instead of

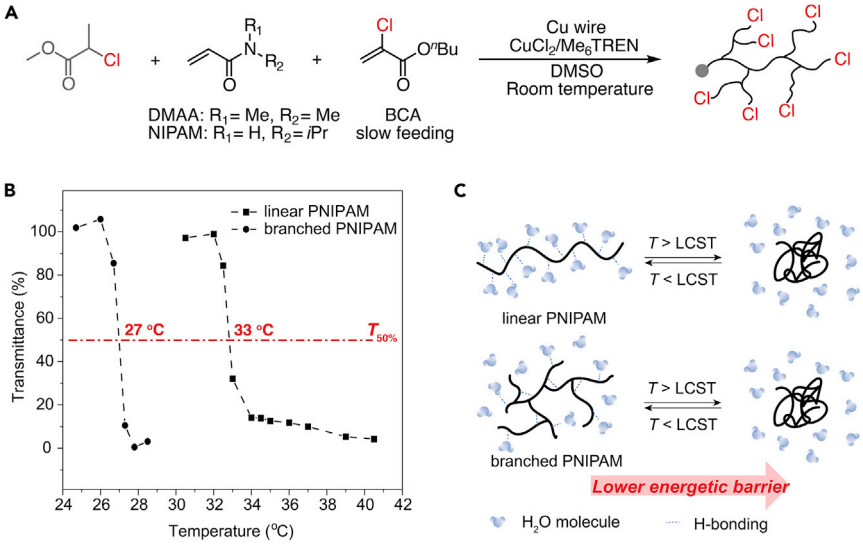

Figure 3. Synthesis of branched PNIPAM and their thermoresponsive behaviors

(A) A representative scheme for the synthesis of branched polyacrylamides via Cu^0-mediated ATRP with Cl-based *inibramer*.

(B and C) (B) LCST of linear and branched PNIPAM in aqueous solution determined by the UV transmittance at 300 nm wavelength and (C) proposed mechanism for the reduced LCST in branched PNIPAM.

$CuBr_2$ to suppress the nucleophilic displacement of the dormant chain end.[96] Cl-based *inibramer*, i.e., *n*-butyl α-chloroacrylate (BCA), was synthesized and employed accordingly. When 4 equiv of BCA was fed at a rate of 0.4 equiv/h (Table 2, entry 2), both DMAA and BCA reached a relatively high conversion in comparison with the homopolymerization of DMAA, and no plateau in the conversion profile was observed (Figure S25A). Poly(*N*,*N*-dimethylacrylamide) (PDMAA) was obtained with $M_{n,GPC}$ and $M_{n,theo}$ of 4.0 and 11.0 kDa, respectively, suggesting the formation of a branched structure. The difference between $M_{n,MALLS}$ and $M_{n,theo}$ can be ascribed to the low initiation efficiency of Cl-based initiators with K_{ATRP} values typically an order of magnitude lower than their Br-based counterparts.[93] When the feed rate of BCA was decreased to 0.2 equiv/h, a lower $Đ$ of 1.94 was obtained (Table 2, entry 3). Increasing the feed ratio of BCA to 8 equiv resulted in a higher DB but also a higher dispersity (Table 2, entry 4). The ^{1}H NMR spectrum of the branched PDMAA indicated the incorporation of both DMAA and BCA (Figure S42), and its ^{13}C NMR spectrum verified the branching junctions derived from the added BCA units (Figure S43). Although incremental success was achieved using Cu^0, we here envision that the utilization of organocatalyzed photo-ATRP can further improve the performance by eliminating the chelating effect of polyacrylamides to the catalyst.[54,99,100]

Finally, *N*-isopropylacrylamide (NIPAM) was successfully copolymerized with BCA in a controlled manner (Table 2, entry 5). The branched poly(*N*-isopropylacrylamide) (PNIPAM) exhibited a decreased lower critical solution temperature (LCST) compared with linear PNIPAM (27°C versus 33°C) (Figure 3B). The branched structure likely facilitated the formation of the intrachain H-bonding in the polymer, lowering its LCST (Figure 3C). Introducing controlled branching opens a facile way to broadening the tuning window of the transition temperature of thermoresponsive polymers. In contrast to the previous strategy of introducing other comonomers to alter the LCST,[101,102] polymers with varied LCST were readily accessed in our work from the same monomer with minimal compositional change.

Please cite this article in press as: Cao et al., Expanding the toolbox of controlled/living branching radical polymerization through simulation-informed reaction design, Chem (2022), https://doi.org/10.1016/j.chempr.2022.02.022

In conclusion, we successfully developed the *inibramer*-mediated activator regeneration ATRP for the synthesis of branched polymers with controlled molecular weight, tunable DB, and relatively low dispersity. Detailed kinetic and mechanistic studies guided us to expand the scope of the monomers and improve the control and livingness in the branching polymerization. The experimental and simulation results demonstrated that both a low Cu concentration and an activator regeneration mechanism played critical roles in achieving a high-conversion polymerization and obtaining branched polymers with high chain end fidelity.

EXPERIMENTAL PROCEDURES

Resource availability

Lead contact

Further information and requests for resources should be directed to and will be fulfilled by the lead contact, Mingjiang Zhong (mingjiang.zhong@yale.edu).

Materials availability

All materials generated in this study are available from the lead contact without restriction.

Data and code availability

All data needed to support the conclusions of this manuscript are included in the main text or supplemental information.

Representative procedure for the photoinitiated ATRP of *n*BA and BBA

An example of photoinitiated ATRP is provided with the following conditions: $[n\text{BA}]_0/[\text{BBA}]_{\text{total}}/[\text{EBiB}]_0/[\text{CuBr}_2]_0/[\text{Me}_6\text{TREN}]_0$ = 300/8/1/0.03/0.18, $[n\text{BA}]_0$ = 4.7 M in DMF at room temperature, feed rate of BBA = 0.8 equiv/h (Table 2, entry 1). To a Schlenk flask equipped with a magnetic stir bar, *n*BA (3.84 g, 30 mmol), DMF (2.0 mL), CuBr_2/DMF solution (25 μL, 0.003 mmol), Me_6TREN (4.8 μL, 0.018 mmol), EBiB (14.7 μL, 0.1 mmol) and propylene carbonate (100 μL, as internal standard to determine conversion by NMR) were added. The mixture was sparged with N_2 for 20 min at 0°C, and then placed into a photoreactor equipped with LED strip with a wavelength of 385–400 nm. Under a stir rate of 500 rpm, the LED light was turned on to initiate the polymerization. 1 h after initiation, a degassed BBA/DMF solution (0.8 M, 1.0 mL) was injected into the flask using a gastight syringe with a syringe pump at a rate of 100 μL/h under N_2 protection. Aliquots were taken using degassed syringes under N_2 flow for ^{1}H NMR and GPC tests. The polymerization lasted for 24 h in total and was quenched by being exposed to air. The resulting polymers were purified by passing through a neutral alumina column followed by preparative GPC.

SUPPLEMENTAL INFORMATION

Supplemental information can be found online at https://doi.org/10.1016/j.chempr.2022.02.022.

ACKNOWLEDGMENTS

M.Z. is thankful for the financial support from National Science Foundation (CHE-1845184). M.C. was partly supported by a Robert M. Langer Fellowship at Yale University. We thank Prof. Krzysztof Matyjaszewski and Mingkang Sun at Carnegie Mellon University, Prof. Aleksandr Zhukhovitskiy and Benjamin Kruse at University of North Carolina at Chapel Hill, and Prof. W. Mark Saltzman, Jinal Pothupitiya, and Julian Grundler at Yale University for GPC-MALLS analysis. We acknowledge

Prof. Peijun Guo at Yale University for the technical support in our photopolymerization set-ups.

AUTHOR CONTRIBUTIONS

M.C., Y.L., X.Z., F.L., and M.Z. designed the research. M.C., Y.L., X.Z., and F.L. conducted the experiments. M.C. and M.Z. carried out the kinetic simulations. M.C. and M.Z. wrote the paper with other authors' additional input.

DECLARATION OF INTERESTS

The authors declare no competing interests.

Received: November 5, 2021
Revised: January 26, 2022
Accepted: February 23, 2022
Published: March 24, 2022

REFERENCES

1. Gao, H., and Matyjaszewski, K. (2009). Synthesis of functional polymers with controlled architecture by CRP of monomers in the presence of cross-linkers: From stars to gels. Prog. Polym. Sci. *34*, 317–350. https://doi.org/10.1016/j.progpolymsci.2009.01.001.

2. Ren, J.M., McKenzie, T.G., Fu, Q., Wong, E.H.H., Xu, J., An, Z., Shanmugam, S., Davis, T.P., Boyer, C., and Qiao, G.G. (2016). Star polymers. Chem. Rev. *116*, 6743–6836. https://doi.org/10.1021/acs.chemrev.6b00008.

3. Sheiko, S.S., Sumerlin, B.S., and Matyjaszewski, K. (2008). Cylindrical molecular brushes: synthesis, characterization, and properties. Prog. Polym. Sci. *33*, 759–785. https://doi.org/10.1016/j.progpolymsci.2008.05.001.

4. Gao, C., and Yan, D. (2004). Hyperbranched polymers: from synthesis to applications. Prog. Polym. Sci. *29*, 183–275. https://doi.org/10.1016/j.progpolymsci.2003.12.002.

5. Jikei, M., and Kakimoto, M.-A. (2001). Hyperbranched polymers: a promising new class of materials. Prog. Polym. Sci. *26*, 1233–1285. https://doi.org/10.1016/S0079-6700(01)00018-1.

6. Voit, B.I., and Lederer, A. (2009). Hyperbranched and highly branched polymer architectures—synthetic strategies and major characterization aspects. Chem. Rev. *109*, 5924–5973. https://doi.org/10.1021/cr900068q.

7. Zheng, Y.C., Li, S.P., Weng, Z.L., and Gao, C. (2015). Hyperbranched polymers: advances from synthesis to applications. Chem. Soc. Rev. *44*, 4091–4130. https://doi.org/10.1039/c4cs00528g.

8. Bosman, A.W., Janssen, H.M., and Meijer, E.W. (1999). About dendrimers: structure, physical properties, and applications. Chem. Rev. *99*, 1665–1688. https://doi.org/10.1021/cr970069y.

9. Grayson, S.M., and Fréchet, J.M.J. (2001). Convergent dendrons and dendrimers: from synthesis to applications. Chem. Rev. *101*, 3819–3868. https://doi.org/10.1021/cr990116h.

10. Hawker, C.J., and Frechet, J.M.J. (1990). Preparation of polymers with controlled molecular architecture. A new convergent approach to dendritic macromolecules. J. Am. Chem. Soc. *112*, 7638–7647. https://doi.org/10.1021/ja00177a027.

11. Svenson, S., and Tomalia, D.A. (2012). Dendrimers in biomedical applications—reflections on the field. Adv. Drug Deliv. Rev. *64*, 102–115. https://doi.org/10.1016/j.addr.2012.09.030.

12. Lutz, J.-F., Lehn, J.-M., Meijer, E.W., and Matyjaszewski, K. (2016). From precision polymers to complex materials and systems. Nat. Rev. Mater. *1*, 16024. https://doi.org/10.1038/natrevmats.2016.24.

13. Matyjaszewski, K. (2011). Architecturally complex polymers with controlled heterogeneity. Science *333*, 1104–1105. https://doi.org/10.1126/science.1209660.

14. Polymeropoulos, G., Zapsas, G., Ntetsikas, K., Bilalis, P., Gnanou, Y., and Hadjichristidis, N. (2017). 50th Anniversary Perspective: polymers with complex architectures. Macromolecules *50*, 1253–1290. https://doi.org/10.1021/acs.macromol.6b02569.

15. Adronov, A., Gilat, S.L., Fréchet, J.M.J., Ohta, K., Neuwahl, F.V.R., and Fleming, G.R. (2000). Light harvesting and energy transfer in laser-dye-labeled poly(aryl ether) dendrimers. J. Am. Chem. Soc. *122*, 1175–1185. https://doi.org/10.1021/ja993272e.

16. Devadoss, C., Bharathi, P., and Moore, J.S. (1996). Energy transfer in dendritic macromolecules: molecular size effects and the role of an energy gradient. J. Am. Chem. Soc. *118*, 9635–9644. https://doi.org/10.1021/ja961418t.

17. Gilat, S.L., Adronov, A., and Fréchet, J.M.J. (1999). Light harvesting and energy transfer in novel convergently constructed dendrimers. Angew. Chem. Int. Ed. Engl. *38*, 1422–1427. https://doi.org/10.1002/(SICI)1521-3773(19990517)38:10<1422::AID-ANIE1422>3.0.CO;2-V.

18. Wang, P.-W., Liu, Y.-J., Devadoss, C., Bharathi, P., and Moore, J.S. (1996). Electroluminescent diodes from a single component emitting layer of dendritic macromolecules. Adv. Mater. *8*, 237–241. https://doi.org/10.1002/adma.19960080311.

19. Yokoyama, S., Otomo, A., Nakahama, T., Okuno, Y., and Mashiko, S. (2003). Dendrimers for optoelectronic applications. In Dendrimers V: Functional and Hyperbranched Building Blocks, Photophysical Properties, Applications in Materials and Life Sciences, C.A. Schalley and F. Vögtle, eds. (Springer), pp. 205–226. https://doi.org/10.1007/b11012.

20. Arrigo, A., Puntoriero, F., La Ganga, G., Campagna, S., Burian, M., Bernstorff, S., and Amenitsch, H. (2017). Aggregation-induced energy transfer in a Decanuclear Os(II)/Ru(II) polypyridine light-harvesting antenna dendrimer. Chem *3*, 494–508. https://doi.org/10.1016/j.chempr.2017.06.002.

21. Diallo, M.S. (2009). Chapter 11. Water treatment by dendrimer-enhanced filtration: principles and applications. In Nanotechnology Applications for Clean Water, N. Savage, M. Diallo, J. Duncan, A. Street, and R. Sustich, eds. (William Andrew Publishing), pp. 143–155. https://doi.org/10.1016/B978-0-8155-1578-4.50020-2.

22. Fréchet, J.M.J. (2002). Dendrimers and supramolecular chemistry. Proc. Natl. Acad. Sci. USA *99*, 4782–4787. https://doi.org/10.1073/pnas.082013899.

23. Boas, U., and Heegaard, P.M.H. (2004). Dendrimers in drug research. Chem. Soc. Rev. *33*, 43–63. https://doi.org/10.1039/B309043B.

24. Lee, C.C., MacKay, J.A., Fréchet, J.M.J., and Szoka, F.C. (2005). Designing dendrimers for biological applications. Nat. Biotechnol. *23*, 1517–1526. https://doi.org/10.1038/nbt1171.

25. Li, F., Cao, M., Feng, Y., Liang, R., Fu, X., and Zhong, M. (2019). Site-specifically initiated controlled/living branching radical

polymerization: a synthetic route toward hierarchically branched architectures. J. Am. Chem. Soc. *141*, 794–799. https://doi.org/10.1021/jacs.8b12433.

26. Mori, H., Böker, A., Krausch, G., and Müller, A.H.E. (2001). Surface-grafted hyperbranched polymers via self-condensing atom transfer radical polymerization from silicon surfaces. Macromolecules *34*, 6871–6882. https://doi.org/10.1021/ma0019048.

27. Muthukrishnan, S., Erhard, D.P., Mori, H., and Müller, A.H.E. (2006). Synthesis and characterization of surface-grafted hyperbranched Glycomethacrylates. Macromolecules *39*, 2743–2750. https://doi.org/10.1021/ma052575s.

28. Pfaff, A., and Müller, A.H.E. (2011). Hyperbranched Glycopolymer grafted microspheres. Macromolecules *44*, 1266–1272. https://doi.org/10.1021/ma102794z.

29. Schüll, C., and Frey, H. (2013). Grafting of hyperbranched polymers: from unusual complex polymer topologies to multivalent surface functionalization. Polymer *54*, 5443–5455. https://doi.org/10.1016/j.polymer.2013.07.065.

30. Flory, P.J. (1952). Molecular size distribution in three dimensional polymers. VI. Branched polymers containing A—R—Bf-1 type units. J. Am. Chem. Soc. *74*, 2718–2723. https://doi.org/10.1021/ja01131a008.

31. Hawker, C.J., Lee, R., and Frechet, J.M.J. (1991). One-step synthesis of hyperbranched dendritic polyesters. J. Am. Chem. Soc. *113*, 4583–4588. https://doi.org/10.1021/ja00012a030.

32. Kim, Y.H., and Webster, O.W. (1990). Water soluble hyperbranched polyphenylene: "a unimolecular micelle?". J. Am. Chem. Soc. *112*, 4592–4593. https://doi.org/10.1021/ja00167a094.

33. Alfurhood, J.A., Bachler, P.R., and Sumerlin, B.S. (2016). Hyperbranched polymers via RAFT self-condensing vinyl polymerization. Polym. Chem. *7*, 3361–3369. https://doi.org/10.1039/C6PY00571C.

34. Fréchet, J.M.J., Henmi, M., Gitsov, I., Aoshima, S., Leduc, M.R., and Grubbs, R.B. (1995). Self-condensing vinyl polymerization—an approach to dendritic materials. Science *269*, 1080–1083. https://doi.org/10.1126/science.269.5227.1080.

35. Gaynor, S.G., Edelman, S., and Matyjaszewski, K. (1996). Synthesis of branched and hyperbranched polystyrenes. Macromolecules *29*, 1079–1081. https://doi.org/10.1021/ma9513877.

36. Hawker, C.J., Frechet, J.M.J., Grubbs, R.B., and Dao, J. (1995). Preparation of hyperbranched and star polymers by a "living", self-condensing free radical polymerization. J. Am. Chem. Soc. *117*, 10763–10764. https://doi.org/10.1021/ja00148a027.

37. Matyjaszewski, K., Gaynor, S.G., Kulfan, A., and Podwika, M. (1997). Preparation of hyperbranched polyacrylates by atom transfer radical polymerization. 1. Acrylic AB* monomers in "living" radical polymerizations. Macromolecules *30*, 5192–5194. https://doi.org/10.1021/ma970359g.

38. Wang, X., and Gao, H. (2017). Recent progress on hyperbranched polymers synthesized via radical-based self-condensing vinyl polymerization. Polymers *9*, 188. https://doi.org/10.3390/polym9060188.

39. Cao, X., Shi, Y., Gan, W., and Gao, H. (2018). Tandem functionalization in a highly branched polymer with layered structure. Chemistry *24*, 5974–5981. https://doi.org/10.1002/chem.201800683.

40. Ohta, Y., Fujii, S., Yokoyama, A., Furuyama, T., Uchiyama, M., and Yokozawa, T. (2009). Synthesis of well-defined hyperbranched polyamides by condensation polymerization of AB2 monomer through changed substituent effects. Angew. Chem. Int. Ed. Engl. *48*, 5942–5945. https://doi.org/10.1002/anie.200901714.

41. Shi, Y., Graff, R.W., Cao, X., Wang, X., and Gao, H. (2015). Chain-growth click polymerization of AB2 monomers for the formation of hyperbranched polymers with low polydispersities in a one-pot process. Angew. Chem. Int. Ed. Engl. *54*, 7631–7635. https://doi.org/10.1002/anie.201502578.

42. Guan, Z. (2002). Control of polymer topology by chain-walking catalysts. Chemistry *8*, 3086–3092. https://doi.org/10.1002/1521-3765(20020715)8:14<3086::AID-CHEM3086>3.0.CO;2-L.

43. Guan, Z., Cotts, P.M., McCord, E.F., and McLain, S.J. (1999). Chain walking: A new strategy to control polymer topology. Science *283*, 2059–2062. https://doi.org/10.1126/science.283.5410.2059.

44. Sun, G., and Guan, Z. (2010). Cascade chain-walking polymerization to generate large dendritic nanoparticles. Macromolecules *43*, 4829–4832. https://doi.org/10.1021/ma100367q.

45. Hanselmann, R., Hölter, D., and Frey, H. (1998). Hyperbranched polymers prepared via the core-dilution/slow addition technique: computer simulation of molecular weight distribution and degree of branching. Macromolecules *31*, 3790–3801. https://doi.org/10.1021/ma971197r.

46. Istratov, V., Kautz, H., Kim, Y.-K., Schubert, R., and Frey, H. (2003). Linear-dendritic nonionic poly(propylene oxide)-polyglycerol surfactants. Tetrahedron *59*, 4017–4024. https://doi.org/10.1016/S0040-4020(03)00470-8.

47. Marcos, A.G., Pusel, T.M., Thomann, R., Pakula, T., Okrasa, L., Geppert, S., Gronski, W., and Frey, H. (2006). Linear-hyperbranched block copolymers consisting of polystyrene and dendritic poly(carbosilane) block. Macromolecules *39*, 971–977. https://doi.org/10.1021/ma051526c.

48. Sunder, A., Hanselmann, R., Frey, H., and Mülhaupt, R. (1999). Controlled synthesis of hyperbranched polyglycerols by ring-opening multibranching polymerization. Macromolecules *32*, 4240–4246. https://doi.org/10.1021/ma990090w.

49. Corrigan, N., Jung, K., Moad, G., Hawker, C.J., Matyjaszewski, K., and Boyer, C. (2020). Reversible-deactivation radical polymerization (controlled/living radical polymerization): from discovery to materials design and applications. Prog. Polym. Sci. *111*, 101311. https://doi.org/10.1016/j.progpolymsci.2020.101311.

50. Parkatzidis, K., Wang, H.S., Truong, N.P., and Anastasaki, A. (2020). Recent developments and future challenges in controlled radical polymerization: a 2020 update. Chem *6*, 1575–1588. https://doi.org/10.1016/j.chempr.2020.06.014.

51. Lu, Y., Nemoto, T., Tosaka, M., and Yamago, S. (2017). Synthesis of structurally controlled hyperbranched polymers using a monomer having hierarchical reactivity. Nat. Commun. *8*, 1863. https://doi.org/10.1038/s41467-017-01838-0.

52. Lu, Y., and Yamago, S. (2019). One-step synthesis of dendritic highly branched polystyrenes by Organotellurium-mediated copolymerization of styrene and a dienyl telluride monomer. Angew. Chem. Int. Ed. Engl. *58*, 3952–3956. https://doi.org/10.1002/anie.201814566.

53. Lu, Y., and Yamago, S. (2020). Synthesis of structurally controlled, highly branched polymethacrylates by radical polymerization through the design of a monomer having hierarchical reactivity. Macromolecules *53*, 3209–3216. https://doi.org/10.1021/acs.macromol.0c00393.

54. Zhao, Y., Ma, M., Lin, X., and Chen, M. (2020). Photoorganocatalyzed divergent reversible-deactivation radical polymerization towards linear and branched fluoropolymers. Angew. Chem. Int. Ed. Engl. *59*, 21470–21474. https://doi.org/10.1002/anie.202009475.

55. Yamago, S. (2021). Practical synthesis of dendritic hyperbranched polymers by reversible deactivation radical polymerization. Polym. J. *53*, 847–864. https://doi.org/10.1038/s41428-021-00487-x.

56. Cao, M., and Zhong, M. (2021). Chain-growth branching radical polymerization: an inibramer strategy. Polym. Int. https://doi.org/10.1002/pi.6315.

57. Kato, M., Kamigaito, M., Sawamoto, M., and Higashimura, T. (1995). Polymerization of methyl methacrylate with the carbon tetrachloride/Dichlorotris-(triphenylphosphine)ruthenium(II)/Methylaluminum bis(2,6-di-tert-butylphenoxide) initiating system: possibility of living radical polymerization. Macromolecules *28*, 1721–1723. https://doi.org/10.1021/ma00109a056.

58. Matyjaszewski, K. (2012). Atom transfer radical polymerization (ATRP): current status and future perspectives. Macromolecules *45*, 4015–4039. https://doi.org/10.1021/ma3001719.

59. Matyjaszewski, K., and Xia, J. (2001). Atom transfer radical polymerization. Chem. Rev. *101*, 2921–2990. https://doi.org/10.1021/cr940534g.

60. Patten, T.E., and Matyjaszewski, K. (1998). Atom transfer radical polymerization and the synthesis of polymeric materials. Adv. Mater. *10*, 901–915. https://doi.org/10.1002/(SICI)

1521-4095(199808)10:12<901::AID-ADMA901>3.0.CO;2-B.

61. Wang, J.-S., and Matyjaszewski, K. (1995). Controlled/"living" radical polymerization. Atom transfer radical polymerization in the presence of transition-metal complexes. J. Am. Chem. Soc. *117*, 5614–5615. https://doi.org/10.1021/ja00125a035.

62. Buback, M., Egorov, M., Gilbert, R.G., Kaminsky, V., Olaj, O.F., Russell, G.T., Vana, P., and Zifferer, G. (2002). Critically evaluated termination rate coefficients for free-radical polymerization, 1. Macromol. Chem. Phys. *203*, 2570–2582. https://doi.org/10.1002/macp.200290041.

63. De Keer, L., Kilic, K.I., Van Steenberge, P.H.M., Daelemans, L., Kodura, D., Frisch, H., De Clerck, K., Reyniers, M.-F., Barner-Kowollik, C., Dauskardt, R.H., and D'hooge, D.R. (2021). Computational prediction of the molecular configuration of three-dimensional network polymers. Nat. Mater. *20*, 1422–1430. https://doi.org/10.1038/s41563-021-01040-0.

64. Barner-Kowollik, C., and Russell, G.T. (2009). Chain-length-dependent termination in radical polymerization: subtle revolution in tackling a long-standing challenge. Prog. Polym. Sci. *34*, 1211–1259. https://doi.org/10.1016/j.progpolymsci.2009.07.002.

65. Zhu, S., and Hamielec, A.E. (1989). Chain-length-dependent termination for free radical polymerization. Macromolecules *22*, 3093–3098. https://doi.org/10.1021/ma00197a033.

66. Fantin, M., Lorandi, F., Ribelli, T.G., Szczepaniak, G., Enciso, A.E., Fliedel, C., Thevenin, L., Isse, A.A., Poli, R., and Matyjaszewski, K. (2019). Impact of organometallic intermediates on copper-catalyzed atom transfer radical polymerization. Macromolecules *52*, 4079–4090. https://doi.org/10.1021/acs.macromol.9b00870.

67. Ribelli, T.G., Augustine, K.F., Fantin, M., Krys, P., Poli, R., and Matyjaszewski, K. (2017). Disproportionation or combination? The termination of acrylate radicals in ATRP. Macromolecules *50*, 7920–7929. https://doi.org/10.1021/acs.macromol.7b01552.

68. Wang, Y., Soerensen, N., Zhong, M., Schroeder, H., Buback, M., and Matyjaszewski, K. (2013). Improving the "livingness" of ATRP by reducing Cu catalyst concentration. Macromolecules *46*, 683–691. https://doi.org/10.1021/ma3024393.

69. Nakamura, Y., Ogihara, T., and Yamago, S. (2016). Mechanism of Cu(I)/Cu(0)-mediated reductive coupling reactions of bromine-terminated polyacrylates, polymethacrylates, and polystyrene. ACS Macro Lett. *5*, 248–252. https://doi.org/10.1021/acsmacrolett.5b00947.

70. Wang, Y., Zhong, M., Zhu, W., Peng, C.-H., Zhang, Y., Konkolewicz, D., Bortolamei, N., Isse, A.A., Gennaro, A., and Matyjaszewski, K. (2013). Reversible-deactivation radical polymerization in the presence of metallic copper. Comproportionation-disproportionation equilibria and kinetics. Macromolecules *46*, 3793–3802. https://doi.org/10.1021/ma400149t.

71. Ballard, N., Salsamendi, M., Santos, J.I., Ruipérez, F., Leiza, J.R., and Asua, J.M. (2014). Experimental evidence shedding light on the origin of the reduction of branching of acrylates in ATRP. Macromolecules *47*, 964–972. https://doi.org/10.1021/ma4025637.

72. The second-order reduction reaction was simplified to a pseudo-first order reaction with reducing agent in excess.

73. Li, X., Wang, W.-J., Li, B.-G., and Zhu, S. (2011). Kinetics and modeling of solution ARGET ATRP of styrene, butyl acrylate, and methyl methacrylate. Macromol. React. Eng. *5*, 467–478. https://doi.org/10.1002/mren.201100024.

74. Anastasaki, A., Nikolaou, V., Zhang, Q., Burns, J., Samanta, S.R., Waldron, C., Haddleton, A.J., McHale, R., Fox, D., Percec, V., et al. (2014). Copper(II)/tertiary amine synergy in photoinduced living radical polymerization: accelerated synthesis of ω-functional and α,ω-Heterofunctional poly(acrylates). J. Am. Chem. Soc. *136*, 1141–1149. https://doi.org/10.1021/ja411780m.

75. Konkolewicz, D., Schröder, K., Buback, J., Bernhard, S., and Matyjaszewski, K. (2012). Visible light and sunlight photoinduced ATRP with ppm of Cu catalyst. ACS Macro Lett. *1*, 1219–1223. https://doi.org/10.1021/mz300457e.

76. Liarou, E., Anastasaki, A., Whitfield, R., Iacono, C.E., Patias, G., Engelis, N.G., Marathianos, A., Jones, G.R., and Haddleton, D.M. (2019). Ultra-low volume oxygen tolerant photoinduced Cu-RDRP. Polym. Chem. *10*, 963–971. https://doi.org/10.1039/C8PY01720D.

77. Pan, X., Malhotra, N., Simakova, A., Wang, Z., Konkolewicz, D., and Matyjaszewski, K. (2015). Photoinduced atom transfer radical polymerization with ppm-level Cu catalyst by visible light in aqueous media. J. Am. Chem. Soc. *137*, 15430–15433. https://doi.org/10.1021/jacs.5b11599.

78. Pan, X., Tasdelen, M.A., Laun, J., Junkers, T., Yagci, Y., and Matyjaszewski, K. (2016). Photomediated controlled radical polymerization. Prog. Polym. Sci. *62*, 73–125. https://doi.org/10.1016/j.progpolymsci.2016.06.005.

79. Ribelli, T.G., Konkolewicz, D., Bernhard, S., and Matyjaszewski, K. (2014). How are radicals (Re)generated in photochemical ATRP? J. Am. Chem. Soc. *136*, 13303–13312. https://doi.org/10.1021/ja506379s.

80. Magenau, A.J.D., Bortolamei, N., Frick, E., Park, S., Gennaro, A., and Matyjaszewski, K. (2013). Investigation of electrochemically mediated atom transfer radical polymerization. Macromolecules *46*, 4346–4353. https://doi.org/10.1021/ma400869e.

81. Magenau, A.J.D., Strandwitz, N.C., Gennaro, A., and Matyjaszewski, K. (2011). Electrochemically mediated atom transfer radical polymerization. Science *332*, 81–84. https://doi.org/10.1126/science.1202357.

82. Park, S., Chmielarz, P., Gennaro, A., and Matyjaszewski, K. (2015). Simplified electrochemically mediated atom transfer radical polymerization using a sacrificial anode. Angew. Chem. Int. Ed. Engl. *54*, 2388–2392. https://doi.org/10.1002/anie.201410598.

83. Jakubowski, W., and Matyjaszewski, K. (2006). Activators regenerated by electron transfer for atom-transfer radical polymerization of (meth)acrylates and related block copolymers. Angew. Chem. Int. Ed. Engl. *45*, 4482–4486. https://doi.org/10.1002/anie.200600272.

84. Konkolewicz, D., Magenau, A.J.D., Averick, S.E., Simakova, A., He, H., and Matyjaszewski, K. (2012). ICAR ATRP with ppm Cu catalyst in water. Macromolecules *45*, 4461–4468. https://doi.org/10.1021/ma300887r.

85. Min, K., Gao, H., and Matyjaszewski, K. (2007). Use of ascorbic acid as reducing agent for synthesis of well-defined polymers by ARGET ATRP. Macromolecules *40*, 1789–1791. https://doi.org/10.1021/ma0702041.

86. Jakubowski, W., Min, K., and Matyjaszewski, K. (2006). Activators regenerated by electron transfer for atom transfer radical polymerization of styrene. Macromolecules *39*, 39–45. https://doi.org/10.1021/ma0522716.

87. Matyjaszewski, K., Coca, S., Gaynor, S.G., Wei, M., and Woodworth, B.E. (1997). Zerovalent metals in controlled/"living" radical polymerization. Macromolecules *30*, 7348–7350. https://doi.org/10.1021/ma971258l.

88. Mohapatra, H., Kleiman, M., and Esser-Kahn, A.P. (2017). Mechanically controlled radical polymerization initiated by ultrasound. Nat. Chem. *9*, 135–139. https://doi.org/10.1038/nchem.2633.

89. Faucher, S., Okrutny, P., and Zhu, S. (2007). Catalyst solubility and experimental determination of equilibrium constants for heterogeneous atom transfer radical polymerization. Ind. Eng. Chem. Res. *46*, 2726–2734. https://doi.org/10.1021/ie061506e.

90. Babu, G.N., Narula, A., Hsu, S.L., and Chien, J.C.W. (1984). Radiolysis of resist polymers. 1. Poly(methyl α-haloacrylates) and copolymers with methyl methacrylate. Macromolecules *17*, 2749–2755. https://doi.org/10.1021/ma00142a054.

91. Matyjaszewski, K., Jo, S.M., Paik, H.-j., and Shipp, D.A. (1999). An investigation into the CuX/2,2′-bipyridine (X = Br or Cl) mediated atom transfer radical polymerization of acrylonitrile. Macromolecules *32*, 6431–6438. https://doi.org/10.1021/ma9905526.

92. Matyjaszewski, K., Mu Jo, S., Paik, H.-J., and Gaynor, S.G. (1997). Synthesis of well-defined polyacrylonitrile by atom transfer radical polymerization. Macromolecules *30*, 6398–6400. https://doi.org/10.1021/ma9706384.

93. Tang, W., Kwak, Y., Braunecker, W., Tsarevsky, N.V., Coote, M.L., and Matyjaszewski, K. (2008). Understanding atom transfer radical polymerization: effect of ligand and initiator structures on the equilibrium constants. J. Am. Chem. Soc. *130*, 10702–10713. https://doi.org/10.1021/ja802290a.

94. Szafko, J., and Turska, E. (1972). Copolymerization of acrylonitrile and methyl

esters of α-substituted acrylic acids. Makromol. Chem. *156*, 311–320. https://doi.org/10.1002/macp.1972.021560123.

95. Rademacher, J.T., Baum, M., Pallack, M.E., Brittain, W.J., and Simonsick, W.J. (2000). Atom transfer radical polymerization of N,N-Dimethylacrylamide. Macromolecules *33*, 284–288. https://doi.org/10.1021/ma991550o.

96. Teodorescu, M., and Matyjaszewski, K. (1999). Atom transfer radical polymerization of (meth) acrylamides. Macromolecules *32*, 4826–4831. https://doi.org/10.1021/ma990175x.

97. Teodorescu, M., and Matyjaszewski, K. (2000). Controlled polymerization of (meth) acrylamides by atom transfer radical polymerization. Macromol. Rapid Commun. *21*, 190–194. https://doi.org/10.1002/(SICI)1521-3927(200003)21:4<190::AID-MARC190>3.0.CO;2-S.

98. Jones, G.R., Li, Z., Anastasaki, A., Lloyd, D.J., Wilson, P., Zhang, Q., and Haddleton, D.M. (2016). Rapid synthesis of well-defined polyacrylamide by aqueous Cu(0)-mediated reversible-deactivation radical polymerization. Macromolecules *49*, 483–489. https://doi.org/10.1021/acs.macromol.5b01994.

99. Theriot, J.C., Lim, C.-H., Yang, H., Ryan, M.D., Musgrave, C.B., and Miyake, G.M. (2016). Organocatalyzed atom transfer radical polymerization driven by visible light. Science *352*, 1082–1086. https://doi.org/10.1126/science.aaf3935.

100. Treat, N.J., Sprafke, H., Kramer, J.W., Clark, P.G., Barton, B.E., Read de Alaniz, J., Fors, B.P., and Hawker, C.J. (2014). Metal-free atom transfer radical polymerization. J. Am. Chem. Soc. *136*, 16096–16101. https://doi.org/10.1021/ja510389m.

101. Akiyama, H., and Tamaoki, N. (2007). Synthesis and photoinduced phase transitions of poly(N-isopropylacrylamide) derivative functionalized with terminal azobenzene units. Macromolecules *40*, 5129–5132. https://doi.org/10.1021/ma070628v.

102. Jochum, F.D., and Theato, P. (2013). Temperature- and light-responsive smart polymer materials. Chem. Soc. Rev. *42*, 7468–7483. https://doi.org/10.1039/C2CS35191A.

Chem, Volume *8*

Supplemental information

Expanding the toolbox of controlled/living branching radical polymerization through simulation-informed reaction design

Mengxue Cao, Yutong Liu, Xiaowei Zhang, Feng Li, and Mingjiang Zhong

I. Supplemental Experimental Procedures

1 General information

Materials: All chemicals were used as received from Sigma Aldrich, Acros Organics, Alfa Aesar, or TCI unless otherwise specified. ACS grade solvents were used as received from Sigma Aldrich and Macron Fine Chemicals. Neutral and basic aluminum oxide (Al_2O_3) (standard activity I grade) were purchased from Sorbent Technologies, Inc. (Sorbtech) with 50–200 μm particle size. Silica gel was purchased from Sorbtech (standard grade) with 60 Å porosity and 40–63 μm particle size. All commercial monomers used in this work were passed through a short column of basic Al_2O_3 to remove inhibitor prior to use. *n*-Butyl α-bromoacrylate (BBA) was synthesized according to previously reported method.[1] HPLC grade anhydrous tetrahydrofuran (THF) and dichloromethane (DCM) were obtained from a J.C. Meyer solvent purification system. Pt gauze (100 mesh woven from 0.0762 mm diameter wire, 99.9%), Pt wire (0.25 mm diameter, 99.9%), and Ag wire (1.0 mm diameter, Premion® 99.999%) were purchased from Alfa Aesar. SHPODA LED light strip (385–400 nm wavelength, 12 V) was purchased from Amazon.

Purification: Flash column chromatography was performed manually or on a Biotage Isolera Prime flash purification system using silica gel. Analytical thin layer chromatography (TLC) was performed on Merck precoated TLC plates (silica gel 60 GF254, 0.25 mm). Preparative gel permeation chromatography (GPC) was performed on a LaboACE LC-5060 recycling preparative HPLC with refractive index (RI) and UV detectors, equipped with a JAIGEL-2.5HR column from Japan Analytical Industry Co., Ltd., operating at a flow rate of 10 mL/min at room temperature. The solvent for the preparative GPC was HPLC grade chloroform from J. T. Baker.

Characterizations: If not particularly mentioned, analytic GPC measurements were taken at a concentration of 0.1–1.0 mg/mL in HPLC grade THF or DMF (J. T. Baker or Fisher) on a Tosoh Bioscience EcoSEC HKC08320 GPC with an RI detector, equipped with a TSKgel GMHHR-M column. The GPC was run at a flow rate of 1.0 mL/min at 40 °C, and the instrument was calibrated using linear monodisperse polystyrene (Sigma Aldrich), poly(methyl methacrylate) (Sigma Aldrich), or poly(ethylene oxide) (Agilent) standards. Analytic GPC with a light scattering detector was performed using two Shodex KD-806M GPC columns connected in series with a DAWN EOS multi-angle laser light scattering (MALLS with 18 angles) detector (Wyatt Technology) and a T-rEX refractive index detector (Wyatt S6 Technology). Experiments were performed at 45 °C using THF or LiBr/DMF (10 mM) eluent at a flow rate of 1 mL/min. Molecular weights were calculated based on d*n*/d*c* values that were obtained assuming 100% mass elution from the columns. ^{1}H NMR spectra were recorded on an Agilent DD2 400 MHz spectrometer and an Agilent DD2 600 MHz spectrometer with 10 s relaxation time. Chemical shifts are reported in ppm using solvent resonance as the internal standard. Data are reported as follows: chemical shift, multiplicity (s = singlet, d = doublet, t = triplet, q = quartet, m = multiplet, dd = doublet of doublets, ddd = doublet of doublet of doublets) coupling constants (Hz), and integration. ^{13}C NMR spectra were recorded on an Agilent DD2 600 MHz spectrometer (150 MHz) spectrometer with complete proton decoupling with 30 s relaxation time. $CDCl_3$, D_2O, and DMSO-d_6 were purchased from Cambridge Isotope Laboratories, Inc. NMR spectra were processed using MestReNova 10.0.1. Lower critical solvent temperatures (LCSTs) of the polymers were determined in an aqueous solution (~30 mg/mL) with a temperature ramp of +0.25 °C/min on a UV-VIS Shimadzu UV-3600Plus. GC-MS was recorded on an Agilent 7200 GC-QTOF system.

General electrochemical set-ups: All electrochemical experiments were conducted at 40 °C, with a Solartron SI 1287 Electrochemical Interface. Measurements were carried out under a N_2 atmosphere using a Pt mesh (~1 cm^2) working electrode (WE), a Pt (wire)/tetrabutylammonium perchlorate ($TBAClO_4$) (0.1 M)/DMF counter electrode (CE), and an Ag (wire)/tetrabutylammonium iodide (TBAI) (0.1 M)/DMF reference electrode (RE). The WE was directly inserted into the reaction solution, and the CE and RE were separated from the solution by a Tylose® gel salt bridge.

Photoreactors: The photoreactor (PR) was prepared by swirling the 385–400 nm LED strip on the inner wall of a 400 mL beaker. A fan was equipped during the polymerization for heat release.

2. Methods

Synthesis of ethyl 2,2-dibromopropanoate (EDBP):

Scheme S1. Synthesis of ethyl 2,2-dibromopropanoate

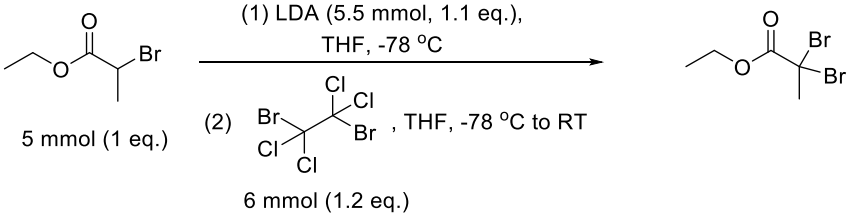

Ethyl 2-bromopropanoate (905 mg, 5.0 mmol) was dissolved in anhydrous THF (10 mL) and immersed into acetone/dry ice bath (–78 °C). LDA (589 mg, 5.5 mmol)/THF (2.0 M) solution was then added into the mixture dropwise. The reaction was stirred for one hour to allow the deprotonation before 1,2-dibromo-1,1,2,2-tetrachloromethane (1.95 g, 6.0 mmol) was added under N_2 protection. The mixture was allowed to be raised slowly to room temperature, and then quenched by adding DI water. The crude product was purified by column chromatography (hexanes/DCM = 4/1 to 3/1) and a yellowish liquid was obtained in 34% yield.

^{1}H NMR (400 MHz, $CDCl_3$) δ 4.34 (q, 2H), 2.65 (s, 3H), 1.36 (t, 3H).

^{13}C NMR (400 MHz, $CDCl_3$) δ 166.96, 63.90, 52.41, 37.44, 13.88.

Synthesis of *n*-butyl α-chloroacrylate (BCA):

Scheme S2. Synthesis of *n*-butyl α-chloroacrylate (BCA)

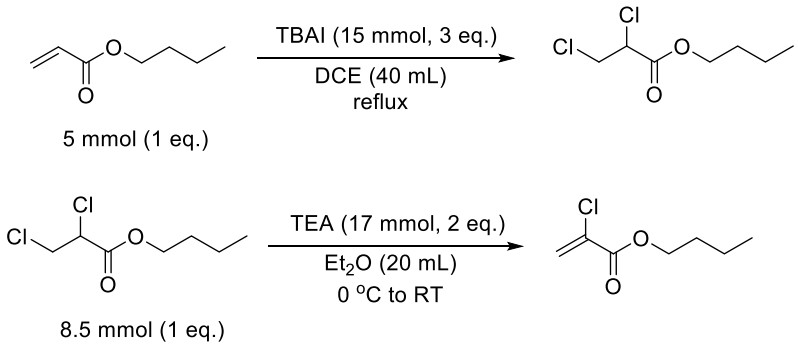

Step 1: Synthesis of *n*-butyl 2,3-dichloropropionate. *n*-Butyl acrylate (0.72 mL, 5.0 mmol) and tetrabutylammonium iodide (5.54 g, 15 mmol) were dissolved in dichloroethane (40 mL) and refluxed for 4 days. The mixture was concentrated under reduced pressure and then diluted with Et_2O (100 mL). The organic phase was washed with aqueous solutions of $NaHSO_3$ (20 wt%), $NaHCO_3$ (saturated), NaCl (saturated), and water successively. After being dried over Na_2SO_4 and concentrated, the crude product was purified by column chromatography (hexanes/EtOAc with EtOAc 0% to 5%) and a colorless liquid was obtained in 28% yield. The final product contains side product BCA.

^{1}H NMR (400 MHz, $CDCl_3$) δ 4.42 (dd, 1H), 4.23 (t, 2H), 3.96 (dd, 2H), 3.80 (dd, 2H), 1.68 (m, 2H), 1.41 (m, 2H), 0.95 (t, 3H).

Step 2: Synthesis of BCA. *n*-Butyl 2,3-dichloropropionate (1.7 g, 8.5 mmol) was dissolved in Et_2O (20 mL). The mixture was cooled to 0 °C and triethylamine (TEA) (2.4 mL, 17 mmol) was added dropwise. The reaction was gradually raised to room temperature and stirred overnight in dark. The salt generated during the reaction was dissolved in water and the aqueous phase was extracted with Et_2O twice. The combined organic phase was dried over Na_2SO_4 and concentrated under reduced pressure. The crude product was purified by column chromatography (hexanes/DCM = 3/1) and a colorless liquid was obtained in 92% yield. BCA was stored in an anisole solution.

^{1}H NMR (400 MHz, $CDCl_3$) δ 6.51 (d, 1H), 6.00 (d, 1H), 4.23 (t, 2H), 1.69 (m, 2H), 1.42 (m, 2H), 0.95 (t, 3H).

Polymerization of *n*BA using different initiators:

An example ATRP of *n*BA is provided with the following conditions: $[n\text{BA}]_0/[\text{EBiB}]_0/[\text{CuBr}]_0/[\text{CuBr}_2]_0/[\text{PMDETA}]_0$ = 200/1/0.6/0.4/1.05, $[n\text{BA}]_0$ = 5.1 M in MeCN (Table S1, entry 1). To a Schlenk flask equipped with a magnetic stir bar, *n*BA (2.56 g, 20 mmol), MeCN (1.0 mL), $CuBr_2$/PMDETA/DMF solution (50 μL, 0.04 mmol/0.105 mmol), and EBiB (14.7 μL, 0.1 mmol) were added. The mixture was degassed by three freeze-pump-thaw cycles and was frozen again. CuBr (8.6 mg, 0.06 mmol) was then added under N_2 protection, and the flask was degassed by evacuation and refill three time. After thawed, the flask was immersed into an oil bath stabilized at 60 °C. Aliquots were taken using degassed syringes under N_2 flow for ^{1}H NMR and GPC tests. The polymerization lasted for 45 hours in total and was quenched by being exposed to air.

Deactivation of the Br-containing carbon-centered free radical:

Scheme S3. Free radical polymerization of BBA and the subsequent deactivation with $CuBr_2$

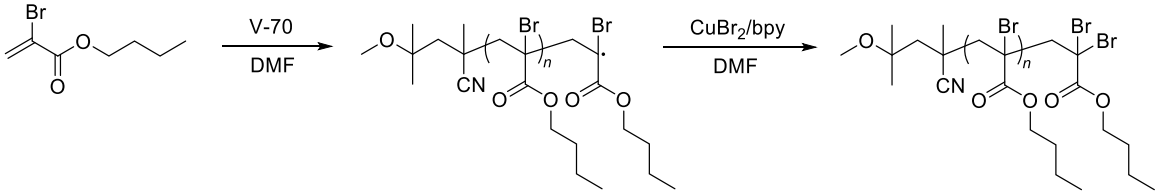

An example of the deactivation experiment is provided with the following conditions: $[\text{BBA}]_0/[\text{V-70}]_0/[\text{CuBr}_2]_0/[\text{bpy}]_0$ = 10/1/40/80 at room temperature, $[\text{V-70}]_0$ = 0.01 M in DMF (Figure S1d). To a Schlenk flask equipped with a magnetic stir bar, 0.01 M 2,2'-azobis(4-methoxy-2,4-dimethyl valeronitrile) (V-70) (15.4 mg, 0.05 mmol), BBA (103.5 mg, 0.5 mmol) and DMF (5.0 mL) were added. The reaction was stirred under N_2 for 3 hours, and $CuBr_2$/bpy/DMF solution (2.0 mmol/4.0 mmol) was then injected. The mixture was exposed to air and stirred to allow the complete deactivation of the propagation radicals. Sample aliquots were taken for ^{13}C NMR analysis.

Copolymerization of *n*BA and BBA via *e*ATRP:

An example of *e*ATRP is provided with the following conditions: $[n\text{BA}]_0/[\text{BBA}]_{\text{total}}/[\text{EBiB}]_0/[\text{CuBr}_2]_0/[\text{Me}_6\text{TREN}]_0$ = 400/8/1/0.4/0.44, $[n\text{BA}]_0$ = 4.4 M in DMF, $[\text{TBAClO}_4]_0$ = 0.1 M, feed rate of BBA = 1.6 equiv./h, *T* = 40 °C, potentiodynamic (Table S4, entry 4). To a multi-neck tapered flask equipped with WE, CE, RE, and a triangle magnetic stir bar, $TBAClO_4$ (0.77 g), DMF (8.0 mL), *n*BA (14.3 mL, 100 mmol), $CuBr_2$/Me_6TREN/DMF solution (1.0 mL, 0.10 mmol/0.11 mmol), and propylene carbonate (200 μL, as internal standard to determine conversion by NMR) were added. The mixture was sparged with N_2 for 20 minutes, and then immersed into an oil bath stabilized at 40 °C. Cyclic voltammetry (CV) was recorded from –0.4 V to 0.8 V versus RE at a scan rate of 50 mV/s while the stir was stopped. EBiB (36.8 μL, 0.25 mmol) was then added under N_2 protection before another CV was recorded. The half potential ($E_{1/2}$) was determined from the CV without EBiB. Under a stir rate of 875 rpm, a potential of $E_{1/2}$ + 80 mV was applied to initiate the polymerization. One hour after initiation, BBA/DMF solution (1.0 M, 2.0 mL) was injected into the flask using a degassed syringe with a syringe pump at a rate of 400 μL/h under N_2 protection. Meanwhile, the applied potential started to decrease at a rate of 3 mV/h until the end of the polymerization. Aliquots were taken using degassed syringes under N_2 flow for ^{1}H NMR and GPC tests. The polymerization lasted for 8 hours in total and was quenched by being exposed to air.

Copolymerization of *n*BA and BBA via photo-ATRP:

An example of photoinitiated ATRP is provided with the following conditions: $[n\text{BA}]_0/[\text{BBA}]_{\text{total}}/[\text{EBiB}]_0/[\text{CuBr}_2]_0/[\text{Me}_6\text{TREN}]_0$ = 300/8/1/0.03/0.18, $[n\text{BA}]_0$ = 4.7 M in DMF at room temperature, feed rate of BBA = 0.8 equiv./h, photoreactor 1 (PR1) (Table 1, entry 1). To a Schlenk flask equipped with a magnetic stir bar, *n*BA (3.84 g, 30 mmol), DMF (2.0 mL), $CuBr_2$/DMF solution (25 μL, 0.003 mmol), Me_6TREN (4.8 μL, 0.018 mmol), EBiB (14.7 μL, 0.1 mmol) and propylene carbonate (100 μL, as internal standard to determine conversion by NMR) were added. The mixture was sparged with N_2 for 20 minutes at 0 °C, and then placed into PR1. Under a stir rate of 500 rpm, the LED light was turned on to initiate the polymerization. One hour after initiation, BBA/DMF solution (0.8 M, 1.0 mL) was injected into the flask using a degassed syringe with a syringe pump at a rate of 100 μL/h under N_2 protection. Aliquots were taken using degassed syringes under N_2 flow for ^{1}H NMR and GPC tests. The polymerization lasted for 24

hours in total and was quenched by exposing to air. The resulting polymers were purified by passing through a neutral alumina column followed by preparative GPC.

Copolymerization of *t*BA and BBA via photo-ATRP:
An example of photoinitiated ATRP is provided with the following conditions: $[tBA]_0/[BBA]_{total}/[EBiB]_0/[CuBr_2]_0/[Me_6TREN]_0$ = 300/16/1/0.03/0.18 at room temperature, $[tBA]_0$ = 4.6 M in DMF, feed rate of BBA = 0.8 equiv./h, photoreactor 1 (PR1) (Table 1, entry 10). To a Schlenk flask equipped with a magnetic stir bar, *t*BA (3.84 g, 30 mmol), DMF (2.0 mL), $CuBr_2$/DMF solution (25 μL, 0.003 mmol), Me_6TREN (4.8 μL, 0.018 mmol), EBiB (14.7 μL, 0.1 mmol) and propylene carbonate (100 μL, as internal standard to determine conversion by NMR) were added. The mixture was sparged with N_2 for 20 minutes at 0 °C, and then placed into PR1. Under a stir rate of 500 rpm, the LED light was turned on to initiate the polymerization. One hour after initiation, BBA/DMF solution (0.8 M, 2.0 mL) was injected into the flask using a degassed syringe with a syringe pump at a rate of 100 μL/h under N_2 protection. Aliquots were taken using degassed syringes under N_2 flow for ^{1}H NMR and GPC tests. The polymerization lasted for 31 hours in total and was quenched by being exposed to air.

Copolymerization of MMA and BBA via photo-ATRP:
An example of photoinitiated ATRP is provided with the following conditions: $[MMA]_0/[BBA]_0/[EBPA]_0/[CuBr_2]_0/[TPMA]_0$ = 300/7/1/0.03/0.18 at room temperature, $[MMA]_0$ = 4.2 M in DMF, photoreactor 2 (PR2) (Table 1, entry 11). To a Schlenk flask equipped with a magnetic stir bar, MMA (3.01 g, 30 mmol), BBA/DMF solution (12.5 wt%, 1.32 g, 0.8 mmol), DMF (2.0 mL), $CuBr_2$/DMF solution (25 μL, 0.003 mmol), TPMA (5.2 mg, 0.018 mmol), EBPA (17.5 μL, 0.1 mmol) and propylene carbonate (100 μL, as internal standard to determine conversion by NMR) were added. The mixture was sparged with N_2 for 20 minutes at 0 °C, and then placed into PR2. Under a stir rate of 500 rpm, the LED light was turned on to initiate the polymerization. Aliquots were taken using degassed syringes under N_2 flow for ^{1}H NMR and GPC tests. The polymerization lasted for 24 hours in total and was quenched by being exposed to air.

Copolymerization of AN and BBA via photo-ATRP:
An example of photoinitiated ATRP is provided with the following conditions: $[AN]_0/[BBA]_{total}/[EBPA]_0/[CuBr_2]_0/[Me_6TREN]_0$ = 300/8/1/0.03/0.18 at room temperature, $[AN]_0$ = 7.2 M in DMSO, feed rate of BBA = 0.8 equiv./h, photoreactor 1 (PR1) (Table 1, entry 13). To a Schlenk flask equipped with a magnetic stir bar, AN (1.59 g, 30 mmol), DMSO (2.0 mL), $CuBr_2$/DMF solution (25 μL, 0.003 mmol), Me_6TREN (4.8 μL, 0.018 mmol), EBPA (17.5 μL, 0.1 mmol) and propylene carbonate (100 μL, as internal standard to determine conversion by NMR) were added. The mixture was sparged with N_2 for 20 minutes at 0 °C, and then placed into PR1. Under a stir rate of 500 rpm, the LED light was turned on to initiate the polymerization. One hour after initiation, BBA/DMF solution (0.8 M, 1.0 mL) was injected into the flask using a degassed syringe with a syringe pump at a rate of 100 μL/h under N_2 protection. Aliquots were taken using degassed syringes under N_2 flow for ^{1}H NMR and GPC tests. The polymerization lasted for 24 hours in total and was quenched by being exposed to air. The resulting polymers were purified by passing through a neutral alumina column followed by precipitation into MeOH/H_2O (1/1, v/v).

Copolymerization of DMAA and BCA via Cu^0-mediated ATRP:
An example of SARA ATRP is provided with the following conditions: $[DMAA]_0/[BCA]_{total}/[MeClPr]_0/[CuCl_2]_0/[Me_6TREN]_0$ = 500/4/1/0.75/1.5 at room temperature, $[DMAA]_0$ = 6.8 M in DMSO, feed rate of BBA = 0.4 equiv./h (Table 2, entry 2). To a Schlenk flask equipped with a magnetic stir bar, DMAA (5.2 mL, 50 mmol), DMSO (2.0 mL), $CuCl_2$/DMF solution (0.2 mL, 0.075 mmol), Me_6TREN (40 μL, 0.15 mmol), and MeClPr (10.8 μL, 0.1 mmol) were added. The mixture was sparged with N_2 for 20 minutes at 0 °C. Under N_2 protection, a Cu wire (d = 1 mm, l = 0.3 cm) was added to initiate the polymerization. Two hours after initiation, BCA/anisole/DMSO solution (0.8 M, 0.5 mL) was injected into the flask using a degassed syringe with a syringe pump at a rate of 50 μL/h under N_2 protection. Aliquots were taken using degassed syringes under N_2 flow for ^{1}H NMR and GPC tests. The polymerization lasted for 34 hours in total and was quenched by being exposed to air. The resulting polymers were purified by passing through a neutral alumina column followed by dialysis with MWCO of 1 kDa against MeOH for 2 days.

Copolymerization of NIPAM and BCA via Cu^0-mediated ATRP:

An example of SARA ATRP is provided with the following conditions: $[NIPAM]_0/[BCA]_{total}/[MeClPr]_0/[CuCl_2]_0/[Me_6TREN]_0$ = 500/4/1/0.75/1.5 at room temperature, $[NIPAM]_0$ = 6.1 M in DMSO, feed rate of BBA = 0.2 equiv./h (Table 2, entry 5). To a Schlenk flask equipped with a magnetic stir bar, NIPAM (5.66 g, 50 mmol), DMSO (8.0 mL), $CuCl_2$/DMF solution (0.2 mL, 0.075 mmol), and Me_6TREN (40 μL, 0.15 mmol) were added. The mixture was sparged with N_2 for 20 minutes at room temperature. Under N_2 protection, MeClPr (10.8 μL, 0.1 mmol) and a Cu wire (*d* = 1 mm, *l* = 0.3 cm) was added to initiate the polymerization. Two hours after initiation, BCA/anisole/DMSO solution (0.8 M, 0.5 mL) was injected into the flask using a degassed syringe with a syringe pump at a rate of 25 μL/h under N_2 protection. Aliquots were taken using degassed syringes under N_2 flow for ^1H NMR and GPC tests. The polymerization lasted for 34 hours and was quenched by being exposed to air.

Synthesis of linear P(NIPAM-*r*-BCA):
To exclude the effect of BCA incorporation in the thermo-responsive behavior of PNIPAM, a linear random copolymer from NIPAM and BCA with the same ratio as that of the branched PNIPAM was synthesized for LCST comparison. Condition: $[NIPAM]_0/[BCA]_0/[AIBN]_0$ = 100/3/1 at 70 °C, $[NIPAM]_0$ = 2.5 M in methanol. NIPAM (565.8 mg, 5.0 mmol), BCA (24.4 mg, 0.15 mmol), and 2,2'-azobis(2-methylpropionitrile) (AIBN) (8.2 mg, 0.05 mmol) were dissolved in methanol (2.0 mL) and degassed with N_2 for 10 minutes. The reaction was immersed into an oil bath at 70 °C and reacted for 20 hours. The reaction was then cooled down and quenched by being exposed to air. Complete conversion was achieved for both monomers.

3. Confirmation of the deactivation of the Br-containing carbon-centered free radical (Scheme 1, A2)

The crude ^{13}C NMR results taken from different deactivation experiments are summarized in Figure S1.

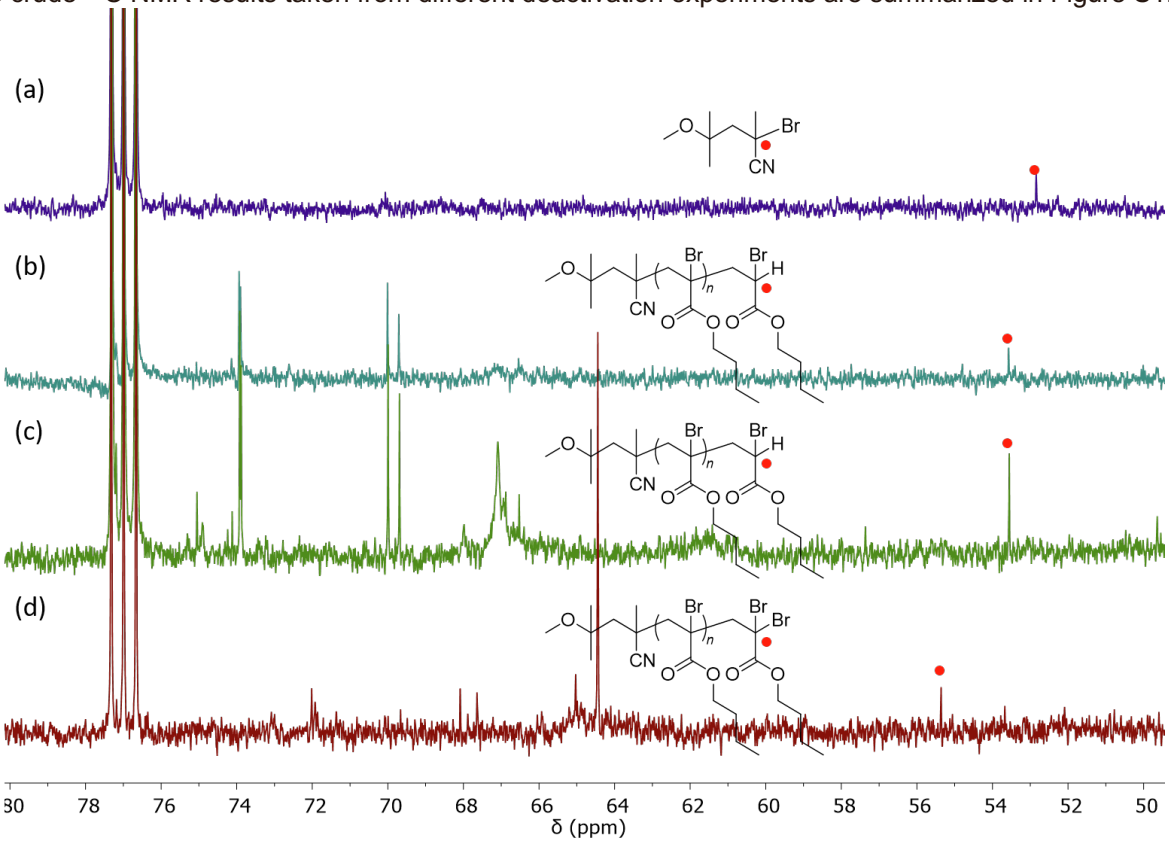

Figure S1. ^{13}C NMR spectra of deactivation reactions (in $CDCl_3$). $[V\text{-}70]_0$ = 0.01 M in DMF, *T* = room temperature. (a) $[V\text{-}70]_0/[CuBr_2]_0/[bpy]_0/[BBA]_0$ = 1/40/80/0. $CuBr_2$ was added at the beginning and the reaction lasted for 5 hours. (b) $[V\text{-}70]_0/[CuBr_2]_0/[bpy]_0/[BBA]_0$ = 1/0/0/10. No $CuBr_2$ was added, and the reaction lasted for 5 hours. (c) $[V\text{-}70]_0/[CuBr_2]_0/[bpy]_0/[BBA]_0$ = 1/40/80/10. $CuBr_2$ was added after 8 hours of polymerization. (d) $[V\text{-}70]_0/[CuBr_2]_0/[bpy]_0/[BBA]_0$ = 1/40/80/10. $CuBr_2$ was added after 3 hours of polymerization.

When BBA was absent, $CuBr_2$/bpy deactivated the radicals generated from V-70 decomposition, resulting in 2-bromonitrile product with tertiary C signal at δ 52.84 ppm (Figure S1a). When $CuBr_2$/bpy deactivator was absent, the free radical polymerization of BBA involved the radical termination. One of the disproportionation products, 2-bromocarboxylate ester, showed the corresponding C signal at δ 53.56 ppm (Figure S1b). When $CuBr_2$/bpy deactivator was added a long period after the initiation, most chain ends still underwent radical termination, resulting in the same result as that with no deactivators (Figure S1c). When $CuBr_2$/bpy deactivator was added after a relatively short time of the initiation and before most propagating chains terminated, the deactivation product, 2,2-dibromocarboxylate ester, was observed in the ^{13}C NMR with the signal at δ 55.36 ppm (Figure S1d).

4. Activation of *gem*-dibromo-species EDBP

Scheme S4. Activation of EDBP in the presence of trapping agents

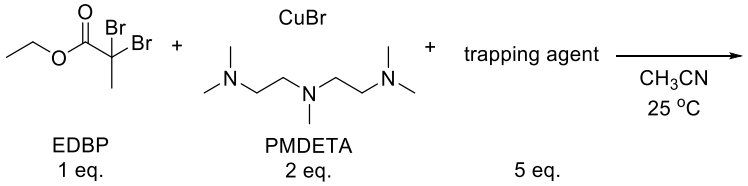

$[EDBP]_0/[CuBr]_0/[PMDETA]_0/[trapping\ agent]_0$ = 1/2/2/5 at room temperature, $[EDBP]_0$ = 0.01 M in MeCN. To a Schleck flask equipped with a magnetic stir bar, EDBP (13.0 mg, 0.05 mmol), PMDETA (17.3 mg, 0.10 mmol), trapping agent (0.25 mmol), and MeCN (2.0 mL) were added. The mixture was degassed with freeze-pump-thaw for three cycles. Under N_2 protection, CuBr (14.3 mg, 0.10 mmol) was added. After 10 min of reaction, crude samples were withdrawn for GC-MS analysis.
Trapping agents: radical trap – TEMPO; carbene trap – benzyl alcohol, 2,3-dimethyl-2-butene.

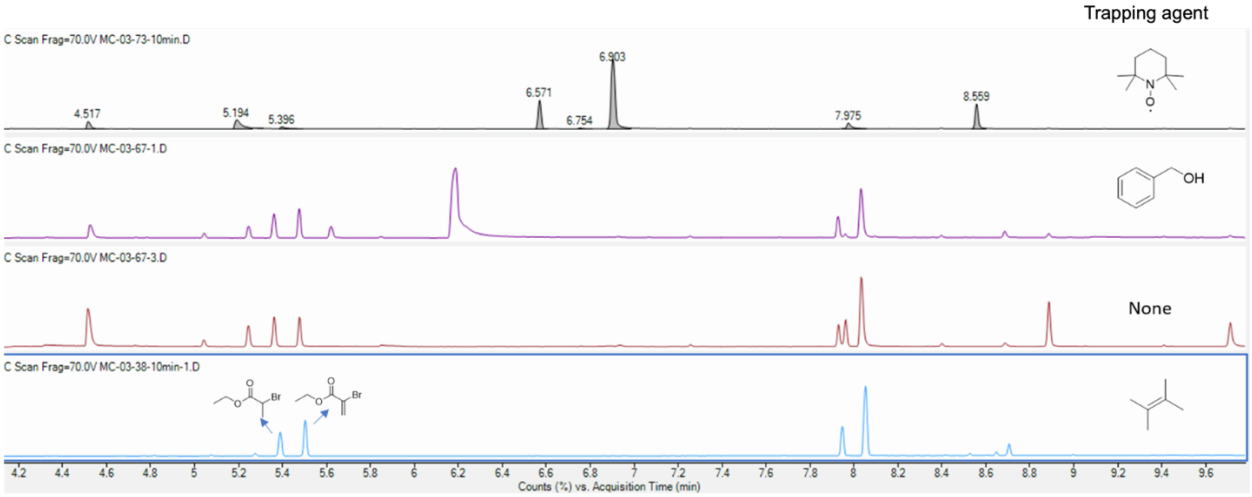

Figure S2. GC-MS profiles of EDBP activation in the presence of different trapping agents.

When no additional agent was added, the crude mixture showed signals for the disproportionation termination products of the bromoradical species.
When radical trap was added, the resulting mixture was significantly different from that where nothing was added. The disappearance of the disproportionation termination products demonstrated the successful trapping when one C–Br bond was activated in EDBP. The molecule after trapping was not observed in GC-MS probably due to the instability of that structure under instrument condition.
When carbene trap was added, the resulting mixture was almost identical to that where nothing was added. Therefore, we reject the possibility that a carbene species forms from the dibromo end when both C–Br bonds were cleaved.

5. Simulations

(i) Estimation of k_a and K_{ATRP}

The activation rate coefficient k_a can be calculated from the activation free energy ($\Delta G^{\neq}$). $\Delta G^{\neq}$ can be related to the R–X bond dissociation energy (BDE) and the Cu–X halogenophilicity ($E(\mathrm{Cu, X\cdot})$) by the two-parameter equation:[2]

$$\Delta G^{\neq}_{\text{predicted}} = 0.56 \times \mathrm{BDE(R-X)} + 0.39 \times E(\mathrm{Cu, X\cdot}) + 4.8 \qquad \textbf{(Eq S1)}$$

The ATRP equilibrium constant K_{ATRP} can be calculated based on the fundamental thermodynamic relation:[3]

$$K_{\text{ATRP}} = K_{\text{BH}} K_{\text{Halo}} \qquad \textbf{(Eq S2)}$$

where K_{BH} and K_{Halo} are directly related to BDE and $E(\mathrm{Cu, X\cdot})$ respectively.

(ii) Estimation of $k_{t,intra}$

Intra-chain termination rate coefficient $k_{t,intra}$ was estimated by fitting the experimental data with EBBiB as initiator to the simulation results.

Scheme S5. ATRP of *n*BA with different initiators

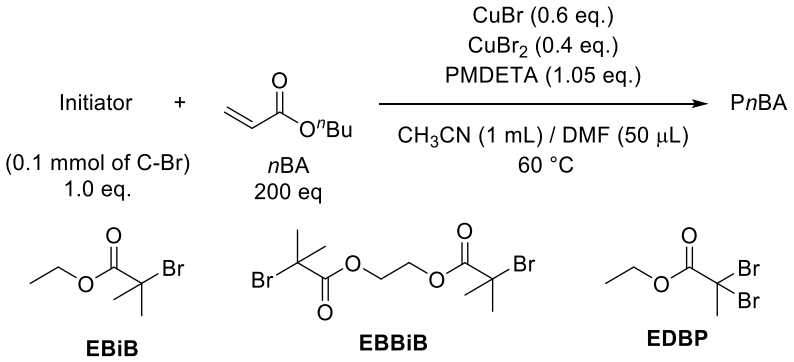

Table S1. ATRP of *n*BA with different initiators (Scheme S5).

Entry	Initiator	*n* (I) (mmol)	Time (h)	Conversion (%)	$M_{n,theo}$ (kDa)	$M_{n,GPC}$ (kDa)	*Đ*
1	EBiB	0.1	45	22.5	6.0	6.1	1.09
2	EBBiB	0.05	45	18.6	9.9	11.5	1.10
3	EDBP	0.05	45	14.0	7.4	10.9	1.10

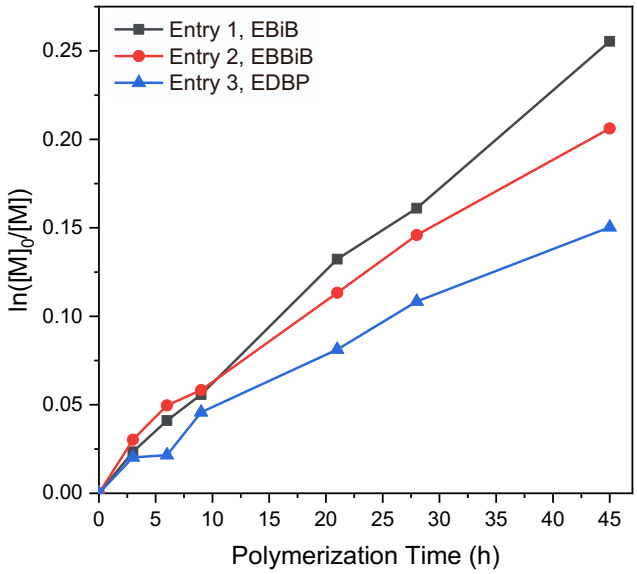

Figure S3. Conversion vs polymerization time of ATRP of *n*BA with different initiators (Table S1).

Table S2. Kinetic model and rate coefficients for conventional ATRP of *n*BA with EBBiB as initiator. [a]

Reaction	Rate coefficient
$\mathrm{R}\cdot + \mathrm{M} \xrightarrow{k_{\mathrm{add}}} \mathrm{P}(1)\cdot$	$k_{\mathrm{add}} = 1.947\times10^{3}\ \mathrm{M^{-1}s^{-1}}$ [b]
$\mathrm{P}(n)\cdot + \mathrm{M} \xrightarrow{k_{\mathrm{p}}} \mathrm{P}(n+1)\cdot$	$k_{\mathrm{p}} = 3.37\times10^{4}\ \mathrm{M^{-1}s^{-1}}$ [c]
$\mathrm{RX} + \mathrm{CuX/L} \xrightarrow{k_{\mathrm{act0}}} \mathrm{R}\cdot + \mathrm{CuX_2/L}$	$k_{\mathrm{act0}} = 8.3\ \mathrm{M^{-1}s^{-1}}$ [d]
$\mathrm{R}\cdot + \mathrm{CuX_2/L} \xrightarrow{k_{\mathrm{deact0}}} \mathrm{RX} + \mathrm{CuX/L}$	$k_{\mathrm{deact0}} = 7.5\times10^{7}\ \mathrm{M^{-1}s^{-1}}$ [e]
$\mathrm{PX}(n) + \mathrm{CuX/L} \xrightarrow{k_{\mathrm{act}}} \mathrm{P}(n)\cdot + \mathrm{CuX_2/L}$	$k_{\mathrm{act}} = 1.02\ \mathrm{M^{-1}s^{-1}}$ [d]
$\mathrm{P}(n)\cdot + \mathrm{CuX_2/L} \xrightarrow{k_{\mathrm{deact}}} \mathrm{PX}(n) + \mathrm{CuX/L}$	$k_{\mathrm{deact}} = 7.7\times10^{8}\ \mathrm{M^{-1}s^{-1}}$ [e]
$\mathrm{R}\cdot + \mathrm{R}\cdot \xrightarrow{k_{\mathrm{t0,intra}}} \mathrm{D0}$	$k_{\mathrm{t0,intra}}$ [f]
$\mathrm{R}\cdot + \mathrm{P}(n)\cdot \xrightarrow{k_{\mathrm{t1,intra}}} \mathrm{D}(n)$	$k_{\mathrm{t1,intra}}$ [f]
$\mathrm{P}(n)\cdot + \mathrm{P}(m)\cdot \xrightarrow{k_{\mathrm{t,intra}}} \mathrm{D}(n+m)$	$k_{\mathrm{t,intra}}$ [f]

[a] Conditions: $[n\mathrm{BA}]_0/[\mathrm{EBBiB}]_0/[\mathrm{CuBr}]_0/[\mathrm{CuBr_2}]_0/[\mathrm{PMDETA}]_0$ = 200/1/0.6/0.4/1.05. $[n\mathrm{BA}]_0$ = 4.0 M in MeCN. T = 60 °C.

[b] k_{add}: the rate coefficient for addition of radicals from EBiB (the same structure as C–Br of EBBiB) to *n*BA. Values are calculated at 60 °C from the frequency factor and activation energy taken from literature.[4,5]

[c] k_{p}: the propagation rate coefficient of *n*BA taken from literature.[6]

[d] k_{act0}, k_{act}: the activation coefficients of EBiB and methyl 2-bromopropionate (MBrP) (the same structure as Br chain end of poly(*n*-butyl acrylate) (P*n*BA)) for ATRP. The systems were first measured at various temperatures and extrapolated to 60 °C according to Arrhenius equation.[7]

[e] k_{deact0}, k_{deact}: the deactivation coefficients of EBiB and P*n*BA chain end calculated from ATRP equilibrium constant (K_{ATRP})[8] and k_{act}. Values for K_{ATRP} for several structural similar Cu catalyst/alkyl halide combinations were previously observed to increase by a factor of 1.5 from room temperature to 60 °C.[9] Values for K_{ATRP} for P*n*BA chain end was estimated by the linear fit of the experimental data using EBiB as initiator (Table S1, entry 1, see the calculation below).

[f] $k_{\mathrm{t0,intra}}$, $k_{\mathrm{t1,intra}}$, $k_{\mathrm{t,intra}}$: the termination rate coefficients involving intrachain termination for small molecule radicals, between a small molecule and a polymeric radical, and for polymeric radicals, respectively. Values were varied to fit the experimental data when using EBBiB as initiator.

Fitting the kinetic data of the early-stage polymerization in Table S1, entry 1 can estimate K_{ATRP} of P*n*BA chain end (Figure S4).

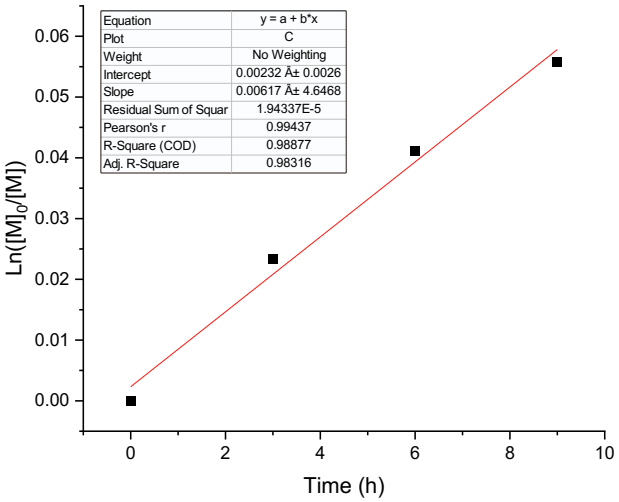

Figure S4. Linear fit of the kinetic data of ATRP of *n*BA (Table S1, entry 1).

$$\ln\left(\frac{[\mathrm{M}]_0}{[\mathrm{M}]}\right) = k_\mathrm{p}[\mathrm{R}\cdot][\mathrm{M}] \Rightarrow k_\mathrm{p}[\mathrm{R}\cdot] = 0.00617\ \mathrm{h}^{-1}$$

$$k_\mathrm{p} = 33700\ \mathrm{mol}^{-1}\cdot\mathrm{s}^{-1} \Rightarrow [\mathrm{R}\cdot] = 5.08\times10^{-11}\ \mathrm{mol}\cdot\mathrm{L}^{-1}$$

$$K_\mathrm{ATRP} = \frac{[\mathrm{R}\cdot][\mathrm{Cu^{II}}]}{[\mathrm{RX}][\mathrm{Cu^{I}}]} = \frac{5.08\times10^{-11}\times0.4}{0.0256\times0.6} = 1.32\times10^{-9}$$

Finding $k_{t,intra}$:

When $k_{t0,intra} \approx k_{t1,intra} \approx k_{t,intra} \approx 2.0\times10^{12}\ M^{-1}s^{-1}$,the early stage of the polymerization fit the simulation results (Figure S5). Later stage of the polymerization was not taken into consideration due to the distance-related intrachain reaction.

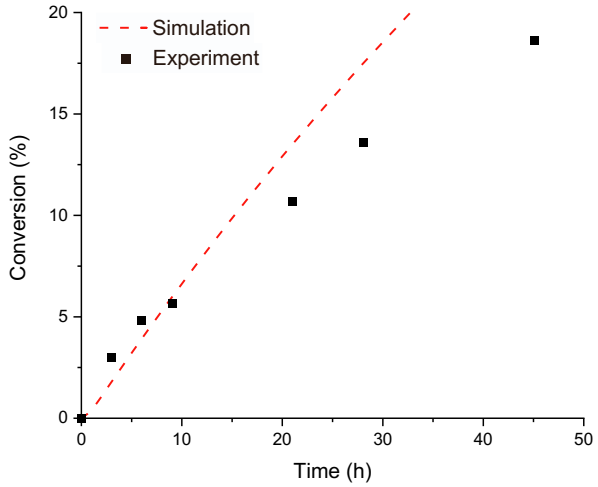

Figure S5. Comparison of simulation and experiment results for conventional ATRP of *n*BA using EBBiB as initiator (Table S1, entry 2).

Considering that the concentration of R· and P(n)· are at the same level for both intermolecular and intramolecular terminations, we conclude that the intrachain termination is 4 orders of magnitude faster than interchain termination, where $k_{t,inter} \sim 10^{-8}\ M^{-1}s^{-1}$.[10]

(iii) Kinetic simulation of copolymerization of *n*BA and BBA via ATRP with or without reducing power

Table S3. Kinetic model and rate coefficients for copolymerization of *n*BA and BBA. [a]

Reaction	Rate coefficient
$R\cdot + M1 \xrightarrow{k_{add1}} P1(1)\cdot$	$k_{add1} = 4.02\times10^{4}\ M^{-1}s^{-1}$ [b]
$R\cdot + M2 \xrightarrow{k_{add2}} P2X(1)\cdot$	$k_{add2} = 1.38\times10^{5}\ M^{-1}s^{-1}$ [b]
$Q\cdot + M1 \xrightarrow{k_{add1}'} P1(1)\cdot$	$k_{add1}' = 1.95\times10^{3}\ M^{-1}s^{-1}$ [b]
$Q\cdot + M2 \xrightarrow{k_{add2}'} P2X(1)\cdot$	$k_{add2}' = 5.91\times10^{3}\ M^{-1}s^{-1}$ [b]
$P1(n)\cdot + M1 \xrightarrow{k_{p11}} P1(n+1)\cdot$	$k_{p11} = 3.37\times10^{4}\ M^{-1}s^{-1}$ [c]
$P1(n)\cdot + M2 \xrightarrow{k_{p12}} P2X(n+1)\cdot$	$k_{p12} = k_{p11}/r_1,\ r_1 = 0.24$ [d]
$P2X(n)\cdot + M1 \xrightarrow{k_{p21}} P1(n+1)\cdot + QX$	$k_{p21} = k_{p22}/r_2,\ r_2 = 9.77$ [c]
$P2X(n)\cdot + M2 \xrightarrow{k_{p22}} P2X(n+1)\cdot + QX$	$k_{p22} = 1.0\times10^{3}\ M^{-1}s^{-1}$ [d]
$RX + CuX/L \xrightarrow{k_{act0}} R\cdot + CuX_2/L$	$k_{act0} = 1.02\ M^{-1}s^{-1}$ [e]
$R\cdot + CuX_2/L \xrightarrow{k_{deact0}} RX + CuX/L$	$k_{deact0} = 1.7\times10^{8}\ M^{-1}s^{-1}$ [f]
$P1X(n) + CuX/L \xrightarrow{k_{act1}} P1(n)\cdot + CuX_2/L$	$k_{act1} = 1.02\ M^{-1}s^{-1}$ [e]
$P1(n)\cdot + CuX_2/L \xrightarrow{k_{deact1}} P1X(n) + CuX/L$	$k_{deact1} = 7.7\times10^{8}\ M^{-1}s^{-1}$ [f]
$P2X2(n) + CuX/L \xrightarrow{k_{act2}} P2X(n)\cdot + CuX_2/L$	$k_{act2} = 8.34\ M^{-1}s^{-1}$ [e]
$P2X(n)\cdot + CuX_2/L \xrightarrow{k_{deact2}} P2X2(n) + CuX/L$	$k_{deact2} = 9.5\times10^{7}\ M^{-1}s^{-1}$ [f]
$QX + CuX/L \xrightarrow{k_{act3}} Q\cdot + CuX_2/L$	$k_{act3} = 8.3\ M^{-1}s^{-1}$ [e]
$Q\cdot + CuX_2/L \xrightarrow{k_{deact3}} QX + CuX/L$	$k_{deact3} = 7.5\times10^{7}\ M^{-1}s^{-1}$ [f]
$R\cdot + R\cdot \xrightarrow{k_{t0}} D0$	$k_{t0} = 2.5\times10^{9}\ M^{-1}s^{-1}$ [g]
$R\cdot + Q\cdot \xrightarrow{k_{t0}} D0$	$k_{t0} = 2.5\times10^{9}\ M^{-1}s^{-1}$ [g]
$Q\cdot + Q\cdot \xrightarrow{k_{t0}'} D0$	$k_{t0}' = 2\times10^{12}\ M^{-1}s^{-1}$ [i]
$R\cdot + P1(n)\cdot \xrightarrow{k_{t1}} D(n)$	$k_{t1} = 5\times10^{8}\ M^{-1}s^{-1}$ [h]
$Q\cdot + P1(n)\cdot \xrightarrow{k_{t1}'} D(n)$	$k_{t1}' = 2\times10^{12}\ M^{-1}s^{-1}$ [i]
$R\cdot + P2X(n)\cdot \xrightarrow{k_{t2}} D(n) + QX$	$k_{t2} = 5\times10^{8}\ M^{-1}s^{-1}$ [h]
$Q\cdot + P2X(n)\cdot \xrightarrow{k_{t2}'} D(n) + QX$	$k_{t2}' = 2\times10^{12}\ M^{-1}s^{-1}$ [i]
$P1(n)\cdot + P1(m)\cdot \xrightarrow{k_{t11}} D(n+m)$	$k_{t11} = 2\times10^{12}\ M^{-1}s^{-1}$ [i]

$\mathrm{P1}(n)\cdot + \mathrm{P2X}(m)\cdot \xrightarrow{k_{t12}} \mathrm{D}(n+m) + \mathrm{QX}$	$k_{t12} = 2\times10^{12}\ \mathrm{M^{-1}s^{-1}}$ [i]
$\mathrm{P2X}(n)\cdot + \mathrm{P2X}(m)\cdot \xrightarrow{k_{t22}} \mathrm{D}(n+m) + 2\mathrm{QX}$	$k_{t22} = 2\times10^{12}\ \mathrm{M^{-1}s^{-1}}$ [i]
$\mathrm{CuX_2/L} \xrightarrow{k_{red}} \mathrm{CuX/L}$	k_{red} [j]

[a] Conditions: $[n\mathrm{BA}]_0/[\mathrm{BBA}]_{total}/[\mathrm{EBP}]_0/[\mathrm{CuBr}]_0/[\mathrm{CuBr_2}]_0/[\mathrm{PMDETA}]_0 = 300/30/1/0.9/0.2/1.1$. $[n\mathrm{BA}]_0 = 4.75$ M in MeCN. $T = 60$ °C. Polymerization lasted for 30 hours. BBA was either added one-pot or slowly fed at a rate of 1.5 equiv./h as a solution with [BBA] = 2.0 M from the beginning of the polymerization. M1 = *n*BA, M2 = BBA. QX = additional initiating points on the backbone originated from the incorporated BBA.

[b] k_{add1}, k_{add2}, k_{add1}', k_{add2}': the rate coefficients for addition of radicals from MBrP to *n*BA, MBrP to MMA (similar structure as BBA), EBiB (similar structure as C–Br on the main chain introduced by BBA) to *n*BA, EBiB to MMA, respectively. Values are calculated at 60 °C from the frequency factor and activation energy taken from literature.[4,5]

[c] k_{p11}, k_{p22}: the propagation rate coefficients of *n*BA and BBA, respectively. k_{p11} was taken from literature.[6] k_{p22} was estimated by fitting the results of free radical polymerization of BBA using 2,2'-azobisisobutyronitrile (AIBN) as initiator at 60 °C and numeric simulation.

[d] r_1, r_2: the reactivity ratios of *n*BA (M1) and BBA (M2) was taken from literature.[11]

[e] k_{act0}, k_{act1}, k_{act2}, k_{act3}: the activation coefficients of EBP, MBrP (the same structure as Br chain end of P*n*BA), BPN (similar bond dissociation energy as EDBP), and EBiB (similar structure as C–Br on the main chain) for ATRP, respectively. The systems were first measured at various temperatures and extrapolated to 60 °C according to Arrhenius equation.[7,12]

[f] k_{deact0}, k_{deact1}, k_{deact2}, k_{deact3}: the deactivation coefficients of EBP, MBrP, BPN, and EBiB, respectively, calculated from K_{ATRP}[8] and k_{act}.

[g] k_{t0}: the termination rate coefficient for small molecule radicals NOT involving intrachain reactions.[13]

[h] k_{t1}, k_{t2}: the termination rate coefficient between a small molecule and a polymeric radical not involving intrachain reactions.[10]

[i] k_{t0}', k_{t1}', k_{t2}', k_{t11}, k_{t12}, k_{t22}: the termination rate coefficients involving intrachain termination for small molecule radicals, between a small molecule and a polymeric radical, and for polymeric radicals.

[j] k_{red}: the reduction rate coefficient for CuX_2/L.

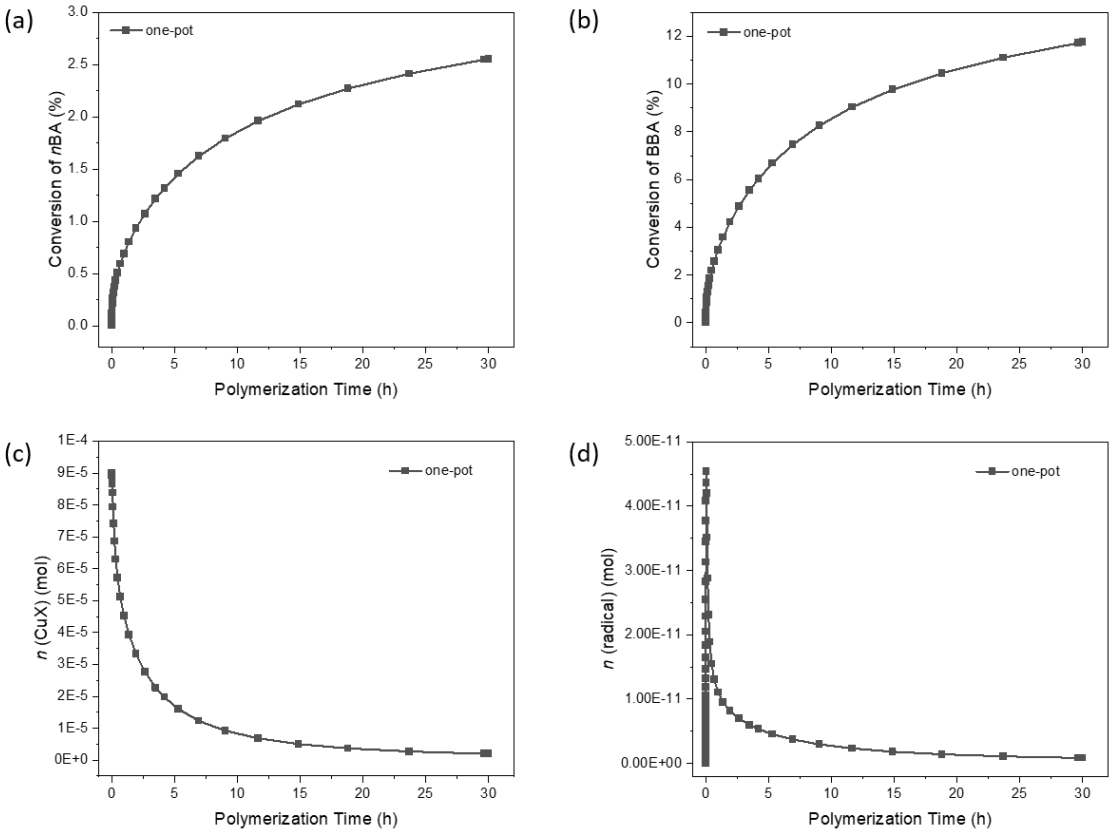

Figure S6. Kinetic simulation of the copolymerization of *n*BA and BBA in one-pot (Figure 1A, one-pot). (a) *n*BA conversion *vs* polymerization time. (b) BBA conversion *vs* polymerization time. (c) activator amount *vs* polymerization time. (d) radical amount *vs* polymerization time.

6. Copolymerization of *n*BA and BBA via *e*ATRP

In a three-electrode setup with a working electrode (WE) of Pt mesh, the semi-batch *e*ATRP of *n*BA and BBA was conducted under an applied potential (E_{app}) with EBiB as the initiator and Me_6TREN as the ligand (Table S4). When 0.04 equiv. of Cu species with respect to the initiator (100 ppm with respect to *n*BA) was introduced into the system, only 16% of *n*BA and 29% of BBA were consumed (Table S4, entry 1). Gelation occurred and spread from the WE to the entire reaction solution, accompanied with the current decay (Figure S7). Hence, the limited accessibility of the gel-embedded WE accounted for the low monomer conversion. A higher Cu concentration was then employed for a more effective activation/deactivation process (Table S4, entry 2–4). By increasing the Cu concentration, a higher conversion and a lower *Đ* were achieved, with suppressed gelation. The current increased first with BBA addition and started to drop when the gelation occurred (Figure S8). The initial increase in current indicated an elevated rate of charge transfer to supply the reduction of $Cu^{II}X/L$ before a steady state was established between the reduction and radical termination. Although utilizing *e*ATRP provided a direct inspection of the $Cu^{II}X/L$ reduction, the mass-transfer limitation of the regenerated activator in such a heterogenous system severely impeded the electro-reduction.

Table S4. Copolymerization of BBA and *n*BA via *e*ATRP.[a]

Entry	[M]/[BBA]/[I]/[$CuBr_2$]	E_{app}[b] (mV)	Time (h)	Feed Rate[c] (eq./h)	Conversion (*n*BA/BBA) (%)	$M_{n,theo}$ (kDa)	$M_{n,GPC}$ (kDa)	$Đ$	S_n
1	400/8/1/0.04	$E_{1/2}$ + 80	8	1.6	16/29	8.6	5.5	1.30	11.1
2	400/8/1/0.1	$E_{1/2}$ + 80	8	1.6	20/40	11.0	9.5	1.20	10.8
3	400/8/1/0.2	$E_{1/2}$ + 80	8	1.6	23/50	12.7	9.6	1.16	10.2
4	400/8/1/0.4	$E_{1/2}$ + 80	8	1.6	17/59	9.8	10.6	1.16	6.5
5	400/8/1/0.4	$E_{1/2}$ + 80 to $E_{1/2}$ + 59[d]	8	1.6	24/56	13.2	10.0	1.16	9.5
6	400/8/1/0.4	$E_{1/2}$ + 80 to $E_{1/2}$ + 45[e]	8	1.6	20/60	11.6	9.3	1.14	7.7
7	400/16/1/0.4	$E_{1/2}$ + 80 to $E_{1/2}$ + 59[d]	8	3.2	17/36	9.9	6.8	1.15	5.4
8	400/24/1/0.4	$E_{1/2}$ + 80 to $E_{1/2}$ + 59[d]	8	4.8	13/38	8.8	6.0	1.20	2.8

[a] Conditions: $[n\text{BA}]_0$ = 4.4 M in DMF at room temperature. $[CuBr_2]_0$/ $[Me_6TREN]_0$ = 1/1.1, $[TBAClO_4]_0$ = 0.1 M, T = 40 °C. [b] Values with respect to the reference electrode. [c] Slow feeding started after one hour of polymerization. [d] Applied potential started to decrease at the rate of 3 mV/h after an hour of polymerization. [e] Applied potential started to decrease at the rate of 5 mV/h after an hour of polymerization.

II. Supplemental Figures

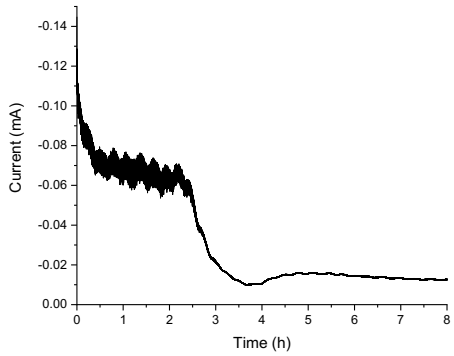

Figure S7. Current *vs* polymerization time in *e*ATRP of *n*BA and BBA (Table S4, entry 1).

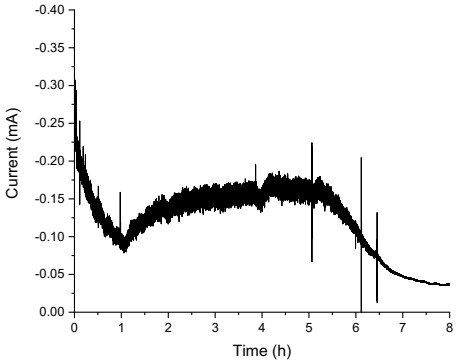

Figure S8. Current *vs* polymerization time in *e*ATRP of *n*BA and BBA (Table S4, entry 3).

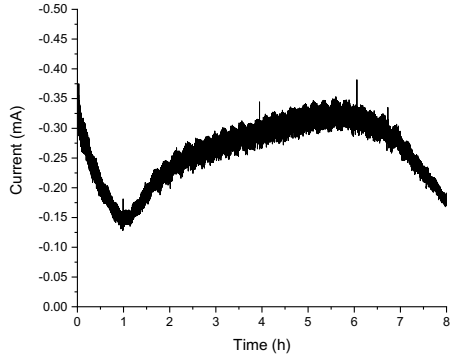

Figure S9. Current *vs* polymerization time in *e*ATRP of *n*BA and BBA (Table S4, entry 5).

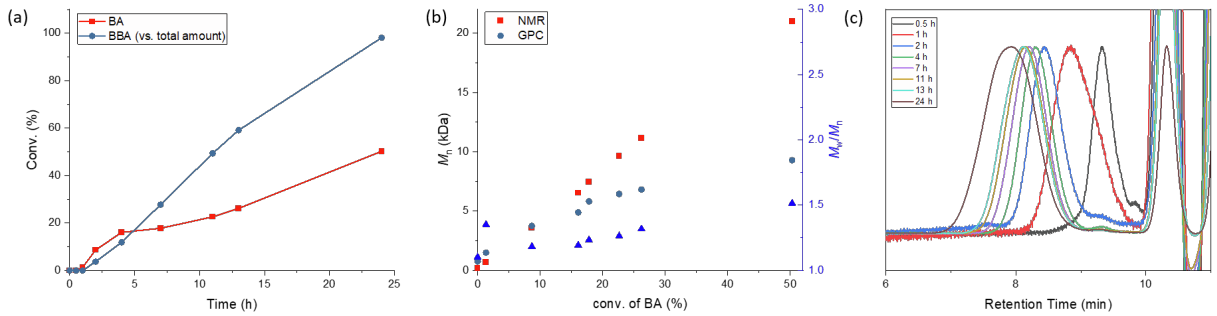

Figure S10. Copolymerization of *n*BA and BBA via photo-ATRP (Table 1, entry 1). (a) Monomer conversion *vs* polymerization time. (b) M_n *vs* *n*BA conversion. (c) GPC traces.

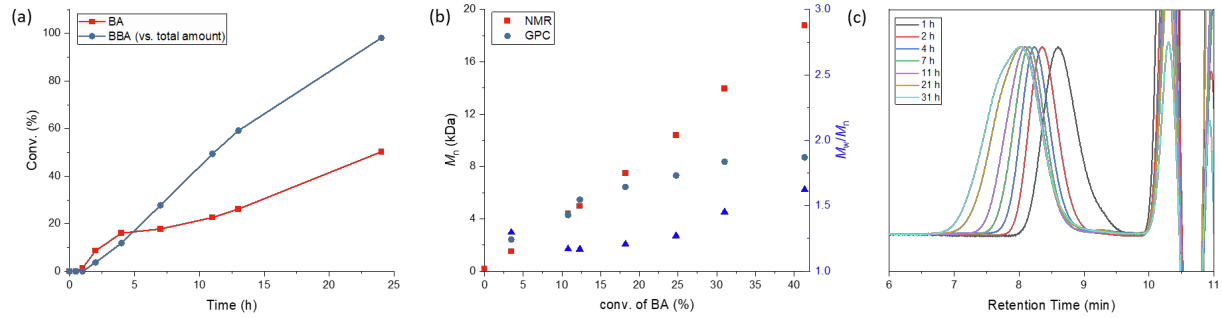

Figure S11. Copolymerization of *n*BA and BBA via photo-ATRP (Table 1, entry 2). (a) Monomer conversion *vs* polymerization time. (b) M_n *vs* *n*BA conversion. (c) GPC traces.

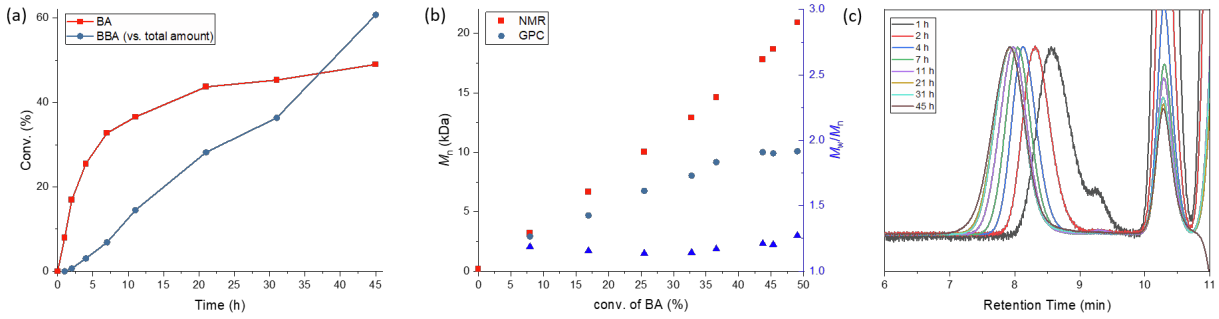

Figure S12. Copolymerization of *n*BA and BBA via photo-ATRP (Table 1, entry 3). (a) Monomer conversion *vs* polymerization time. (b) M_n *vs* *n*BA conversion. (c) GPC traces.

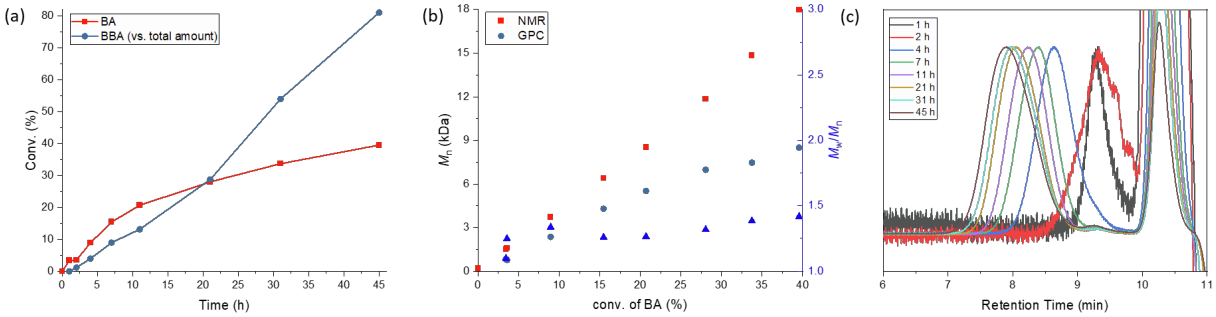

Figure S13. Copolymerization of *n*BA and BBA via photo-ATRP (Table 1, entry 4). (a) Monomer conversion *vs* polymerization time. (b) M_n *vs n*BA conversion. (c) GPC traces.

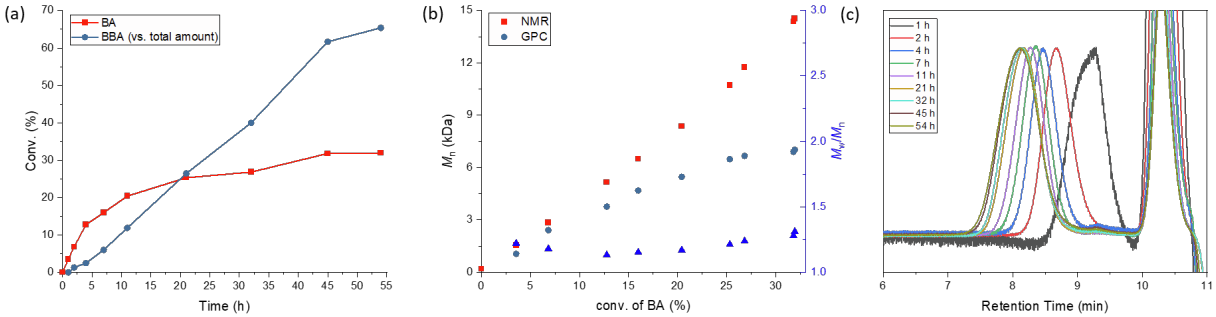

Figure S14. Copolymerization of *n*BA and BBA via photo-ATRP (Table 1, entry 5). (a) Monomer conversion *vs* polymerization time. (b) M_n *vs n*BA conversion. (c) GPC traces.

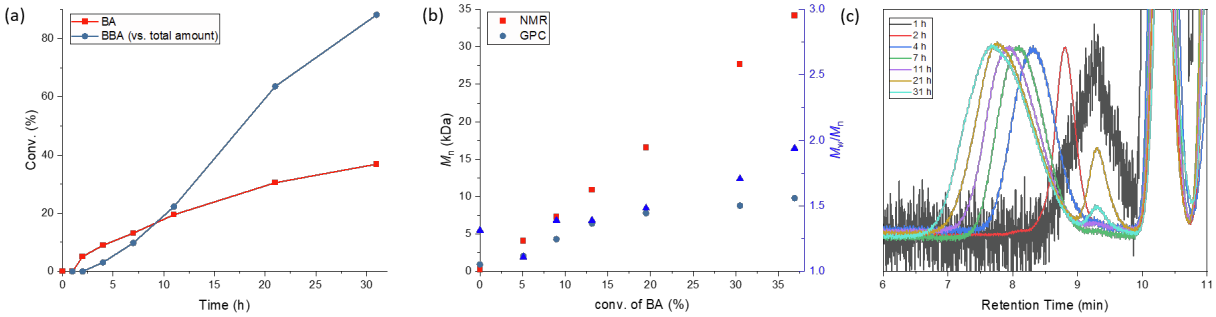

Figure S15. Copolymerization of *n*BA and BBA via photo-ATRP (Table 1, entry 6). (a) Monomer conversion *vs* polymerization time. (b) M_n *vs n*BA conversion. (c) GPC traces.

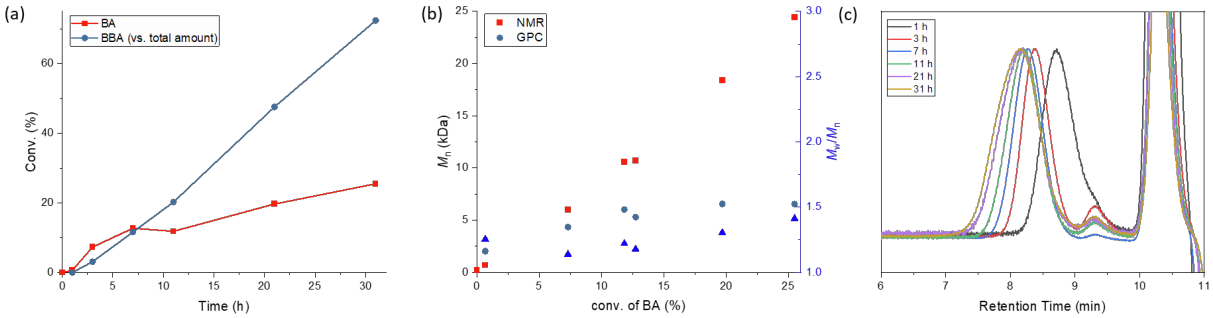

Figure S16. Copolymerization of *n*BA and BBA via photo-ATRP (Table 1, entry 7). (a) Monomer conversion *vs* polymerization time. (b) M_n *vs* *n*BA conversion. (c) GPC traces.

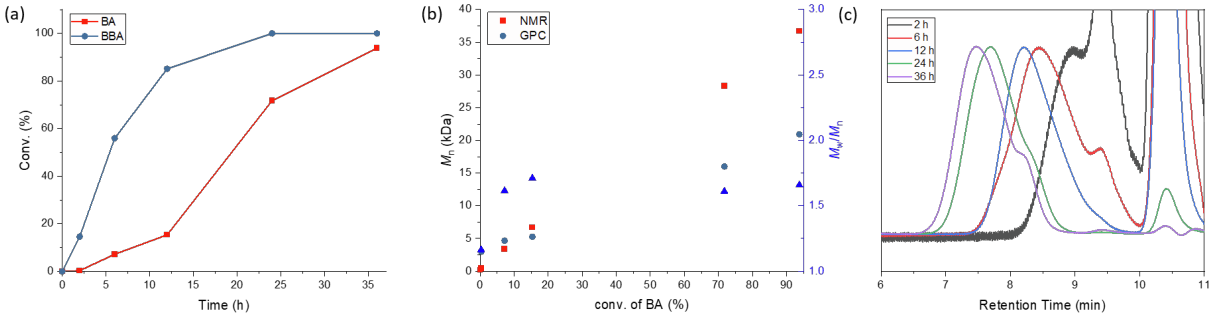

Figure S17. Copolymerization of *n*BA and BBA via photo-ATRP (Table 1, entry 8). (a) Monomer conversion *vs* polymerization time. (b) M_n *vs* *n*BA conversion. (c) GPC traces.

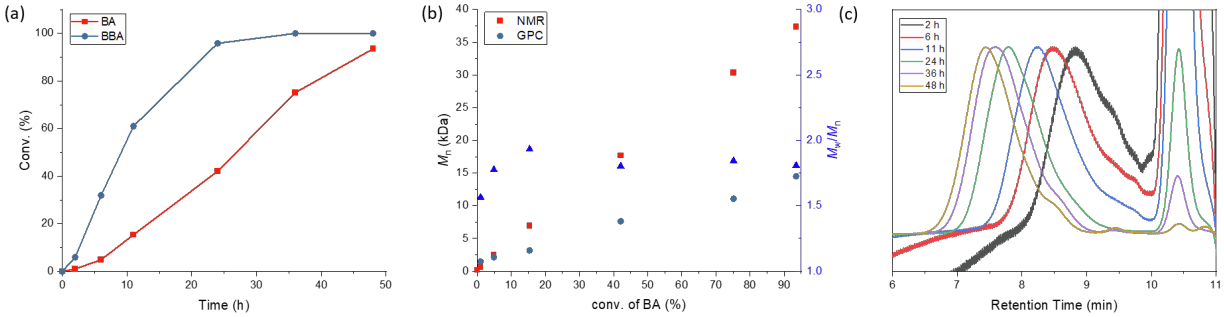

Figure S18. Copolymerization of *n*BA and BBA via photo-ATRP (Table 1, entry 9). (a) Monomer conversion *vs* polymerization time. (b) M_n *vs* *n*BA conversion. (c) GPC traces.

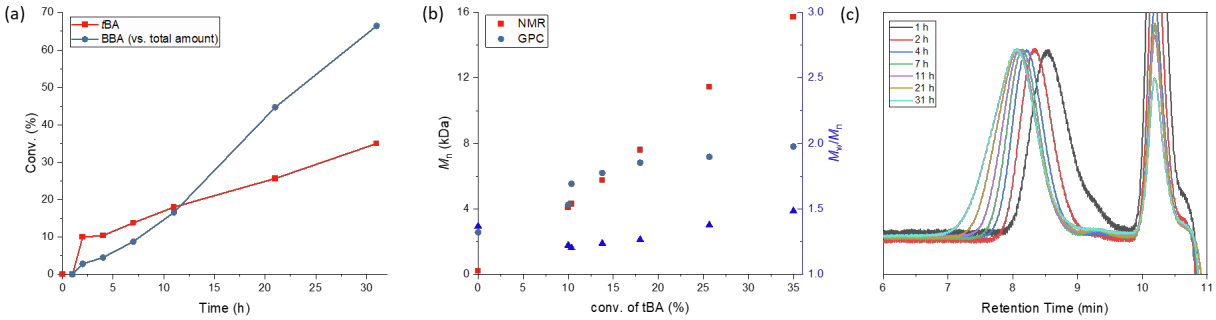

Figure S19. Copolymerization of *t*BA and BBA via photo-ATRP (Table 1, entry 10). (a) Monomer conversion *vs* polymerization time. (b) M_n *vs* *t*BA conversion. (c) GPC traces.

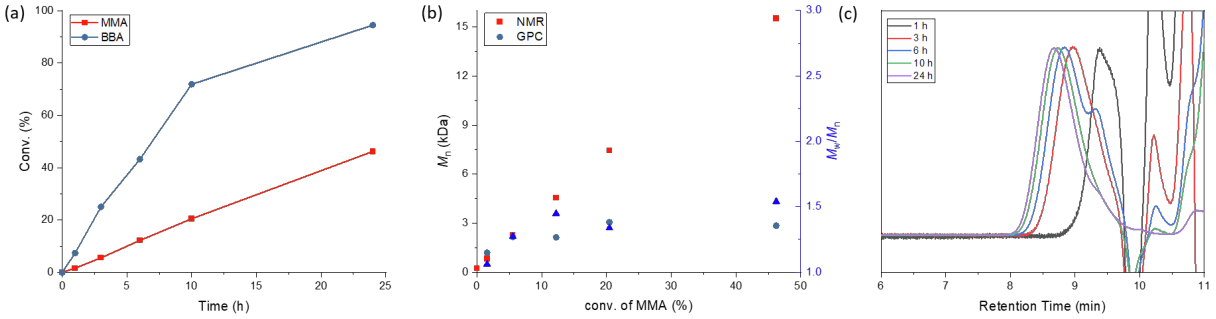

Figure S20. Copolymerization of MMA and BBA via photo-ATRP (Table 1, entry 11). (a) Monomer conversion *vs* polymerization time. (b) M_n *vs* MMA conversion. (c) GPC traces.

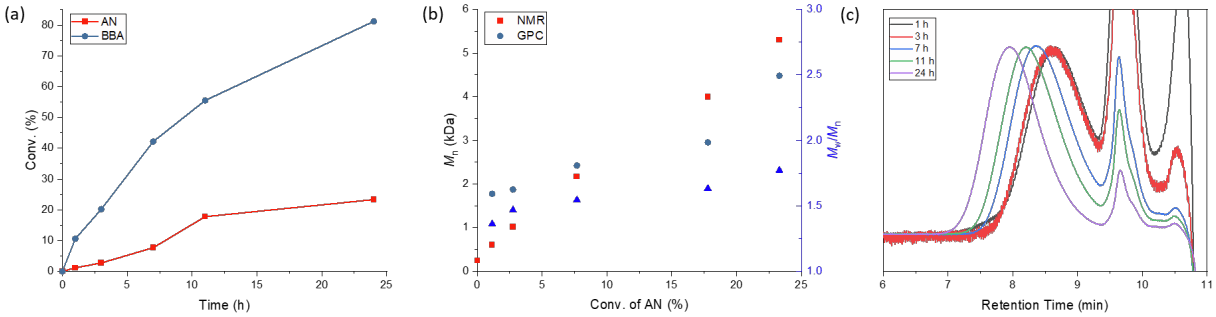

Figure S21. Copolymerization of AN and BBA via photo-ATRP (Table 1, entry 12). (a) Monomer conversion *vs* polymerization time. (b) M_n *vs* AN conversion. (c) GPC traces.

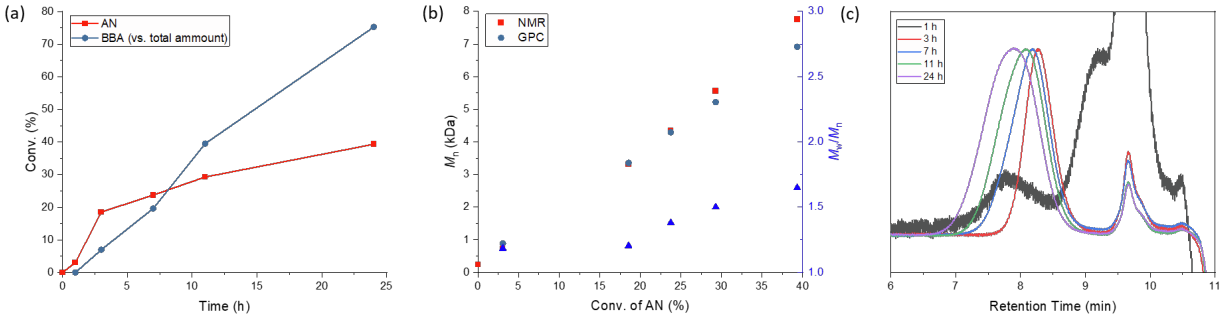

Figure S22. Copolymerization of AN and BBA via photo-ATRP (Table 1, entry 13). (a) Monomer conversion *vs* polymerization time. (b) M_n *vs* AN conversion. (c) GPC traces.

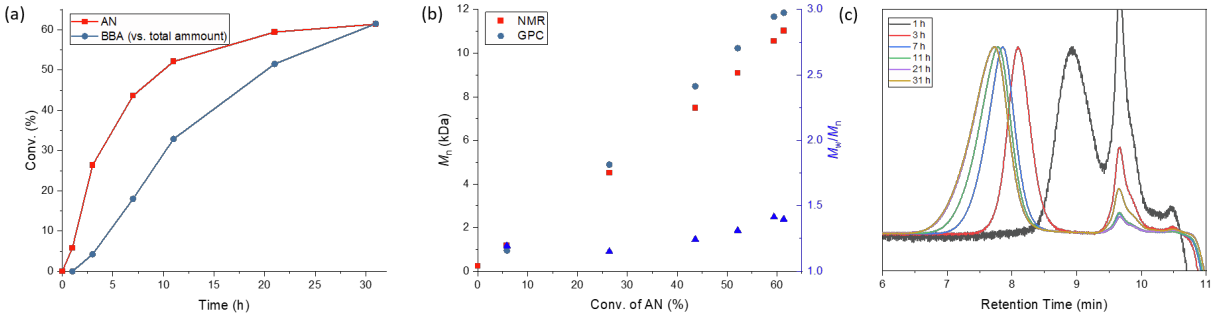

Figure S23. Copolymerization of AN and BBA via photo-ATRP (Table 1, entry 14). (a) Monomer conversion *vs* polymerization time. (b) M_n *vs* AN conversion. (c) GPC traces.

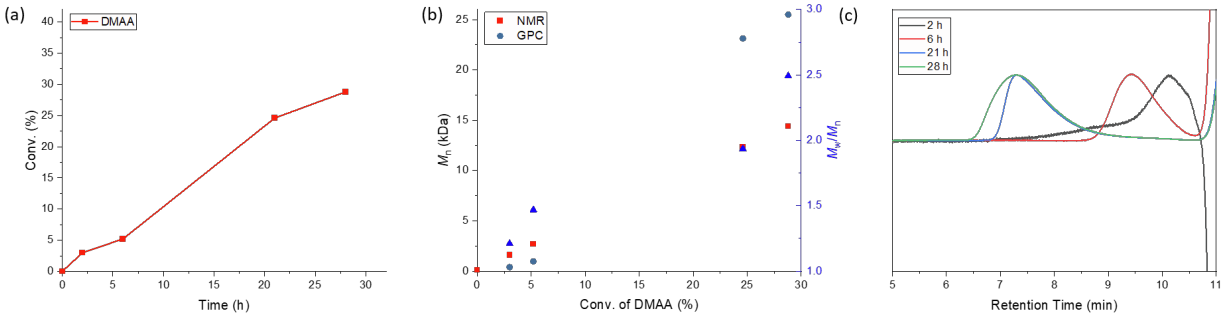

Figure S24. polymerization of DMAA via Cu^0-mediated ATRP (Table 2, entry 1). (a) Monomer conversion *vs* polymerization time. (b) M_n *vs* DMAA conversion. (c) GPC traces.

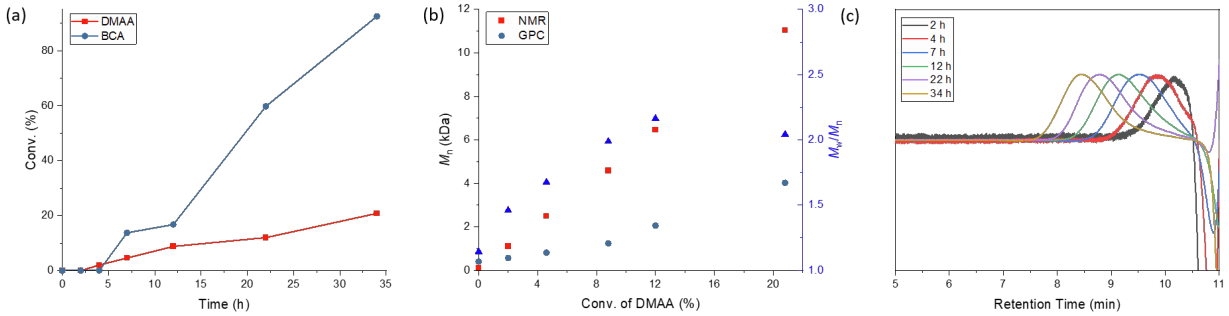

Figure S25. Copolymerization of DMAA and BCA via Cu^0-mediated ATRP (Table 2, entry 2). (a) Monomer conversion *vs* polymerization time. (b) M_n *vs* DMAA conversion. (c) GPC traces.

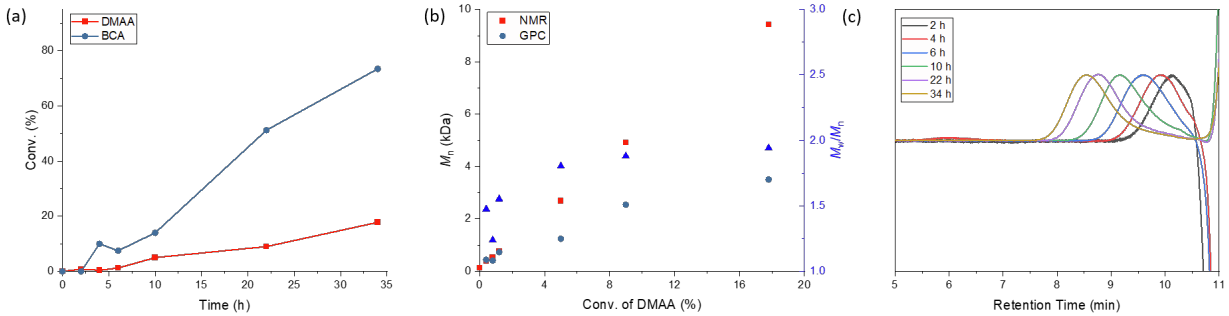

Figure S26. Copolymerization of DMAA and BCA via Cu^0-mediated ATRP (Table 2, entry 3). (a) Monomer conversion *vs* polymerization time. (b) M_n *vs* DMAA conversion. (c) GPC traces.

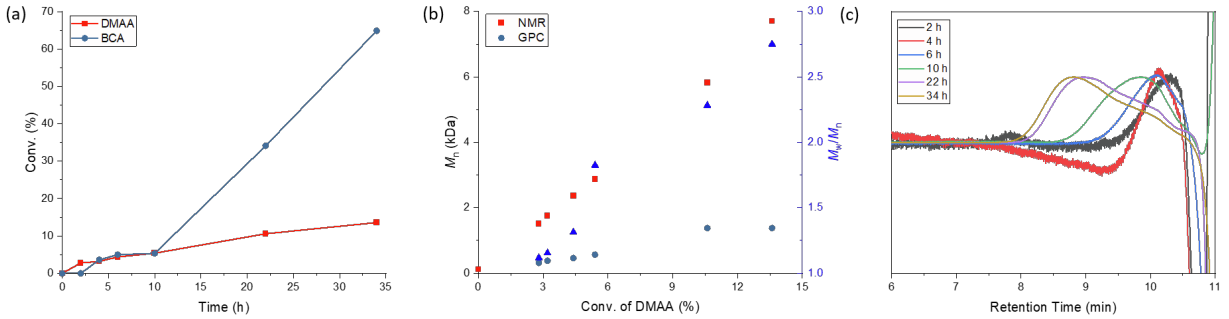

Figure S27. Copolymerization of DMAA and BCA via Cu^0-mediated ATRP (Table 2, entry 4). (a) Monomer conversion *vs* polymerization time. (b) M_n *vs* DMAA conversion. (c) GPC traces.

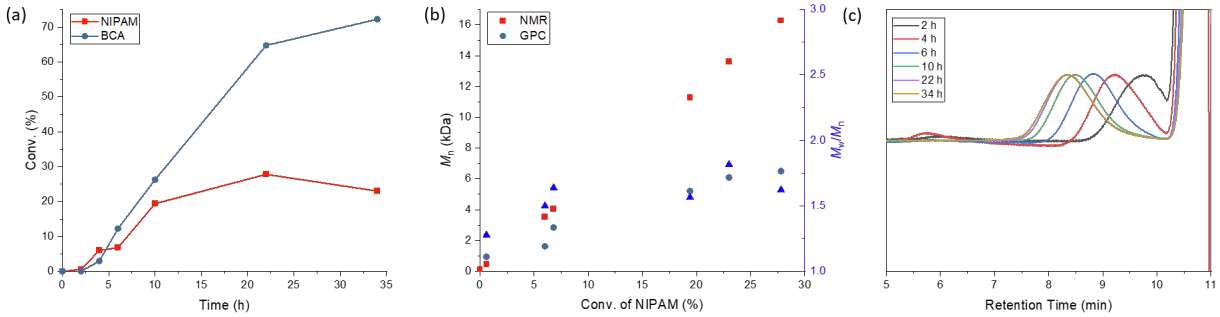

Figure S28. Copolymerization of NIPAM and BCA via Cu^0-mediated ATRP (Table 2, entry 5). (a) Monomer conversion *vs* polymerization time. (b) M_n *vs* NIPAM conversion. (c) GPC traces.

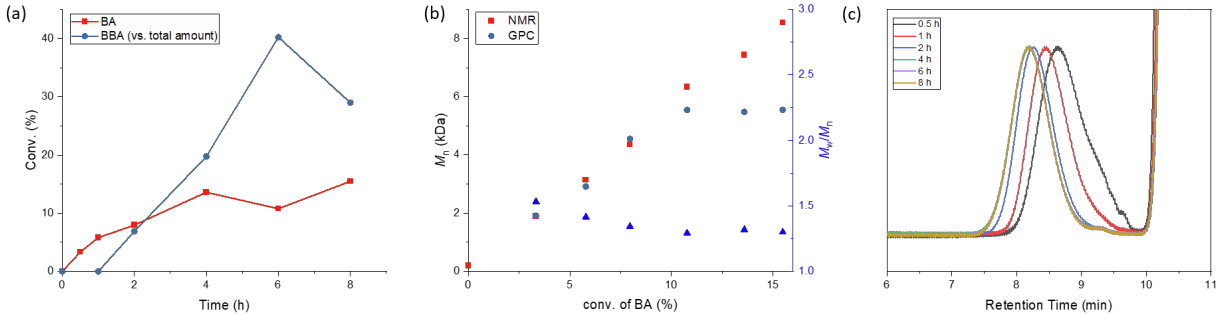

Figure S29. Copolymerization of *n*BA and BBA via *e*ATRP (Table S4, entry 1). (a) Monomer conversion *vs* polymerization time. (b) M_n *vs* *n*BA conversion. (c) GPC traces.

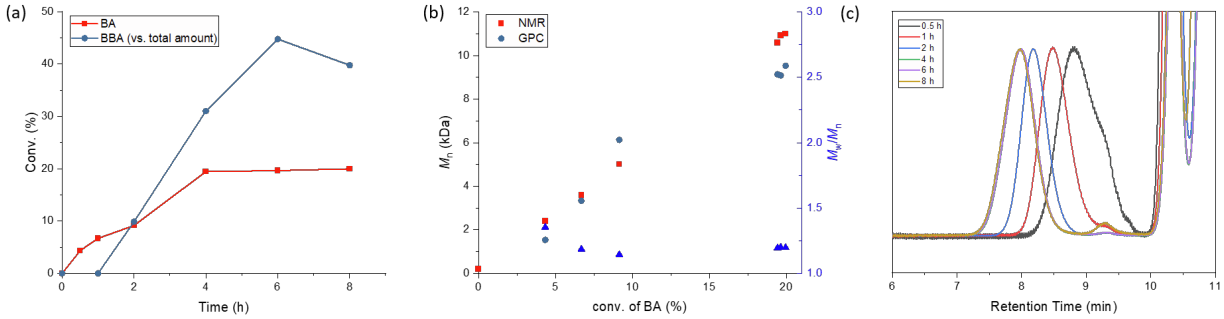

Figure S30. Copolymerization of *n*BA and BBA via *e*ATRP (Table S4, entry 2). (a) Monomer conversion *vs* polymerization time. (b) M_n *vs* *n*BA conversion. (c) GPC traces.

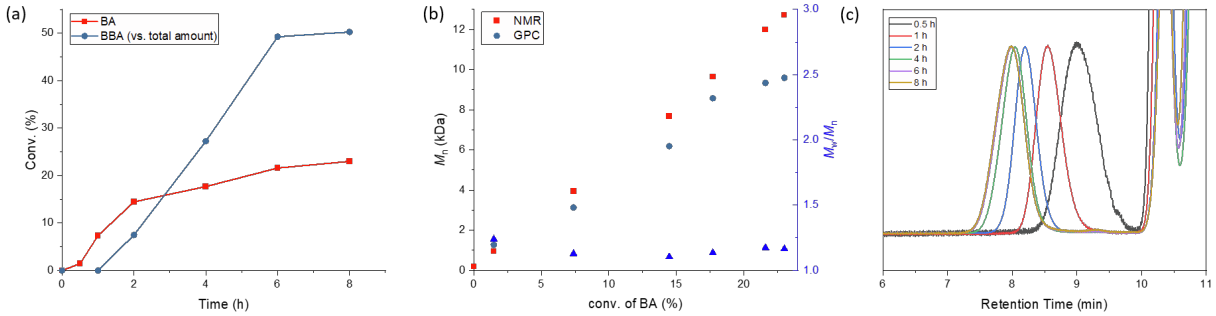

Figure S31. Copolymerization of *n*BA and BBA via *e*ATRP (Table S4, entry 3). (a) Monomer conversion *vs* polymerization time. (b) M_n *vs n*BA conversion. (c) GPC traces.

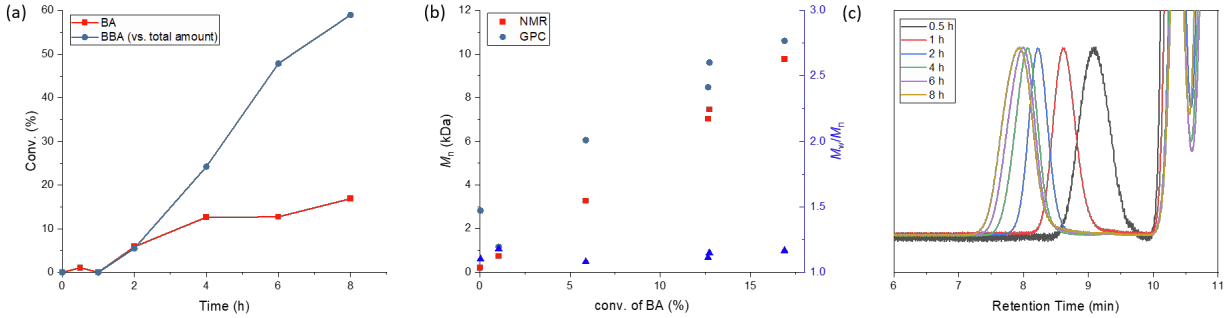

Figure S32. Copolymerization of *n*BA and BBA via *e*ATRP (Table S4, entry 4). (a) Monomer conversion *vs* polymerization time. (b) M_n *vs n*BA conversion. (c) GPC traces.

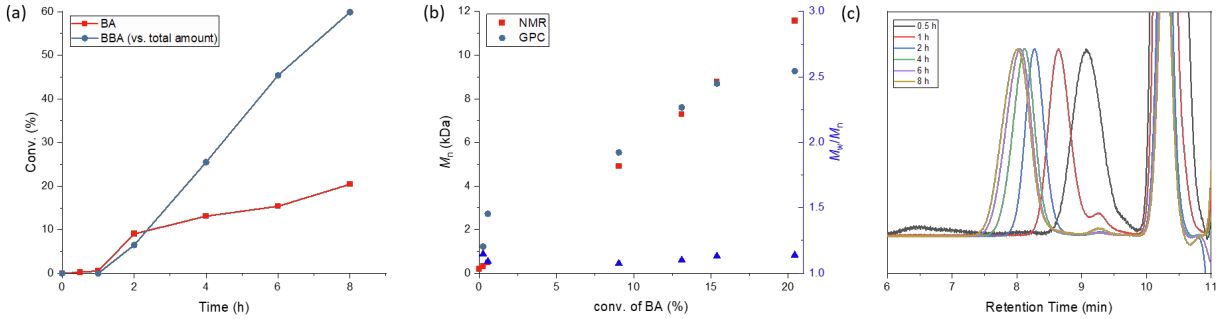

Figure S33. Copolymerization of *n*BA and BBA via *e*ATRP (Table S4, entry 5). (a) Monomer conversion *vs* polymerization time. (b) M_n *vs n*BA conversion. (c) GPC traces.

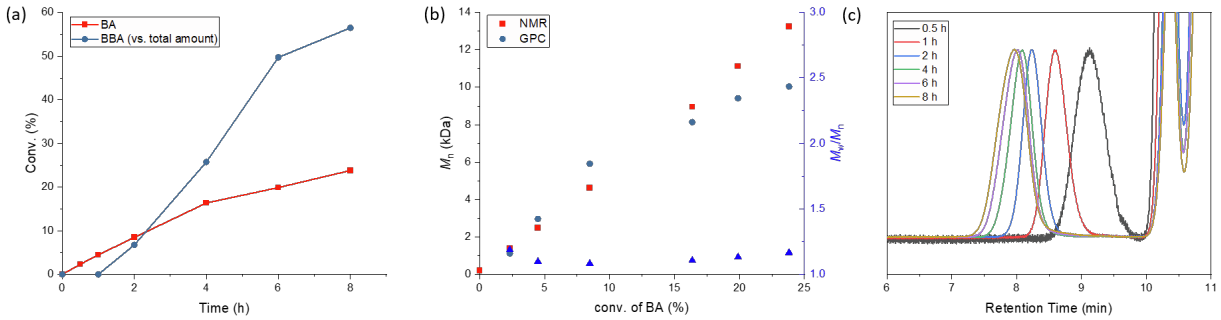

Figure S34. Copolymerization of *n*BA and BBA via *e*ATRP (Table S4, entry 6). (a) Monomer conversion *vs* polymerization time. (b) M_n *vs n*BA conversion. (c) GPC traces.

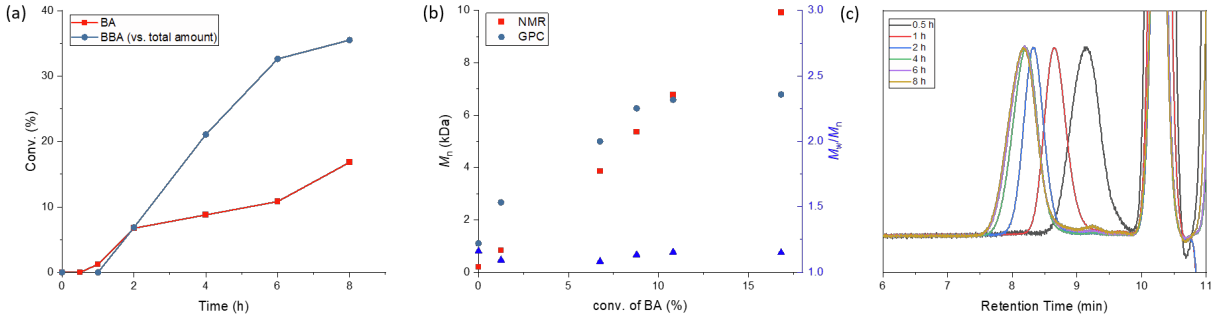

Figure S35. Copolymerization of *n*BA and BBA via *e*ATRP (Table S4, entry 7). (a) Monomer conversion *vs* polymerization time. (b) M_n *vs n*BA conversion. (c) GPC traces.

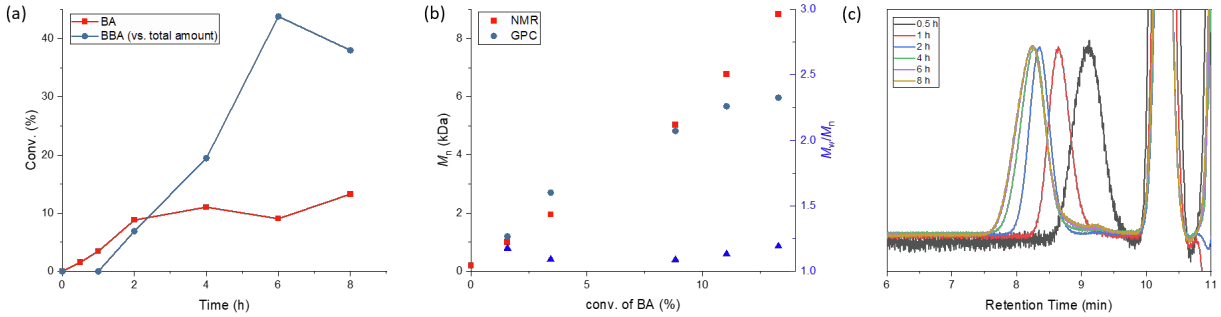

Figure S36. Copolymerization of *n*BA and BBA via *e*ATRP (Table S4, entry 8). (a) Monomer conversion *vs* polymerization time. (b) M_n *vs n*BA conversion. (c) GPC traces.

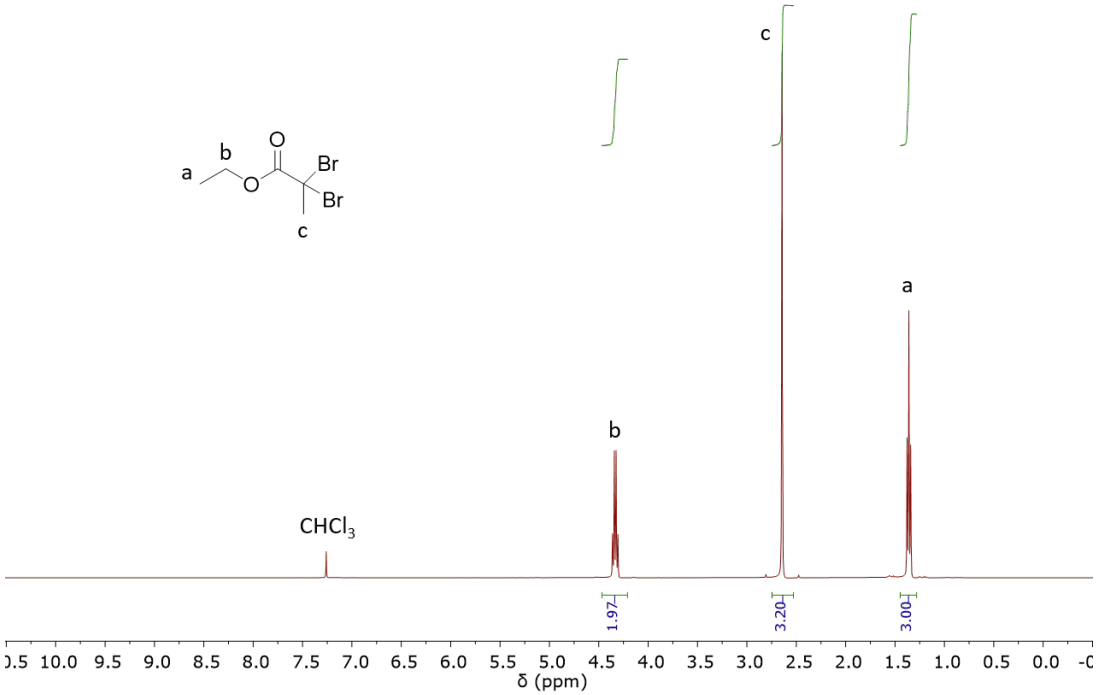

Figure S37. ^{1}H NMR spectrum of EDBP (in $CDCl_3$).

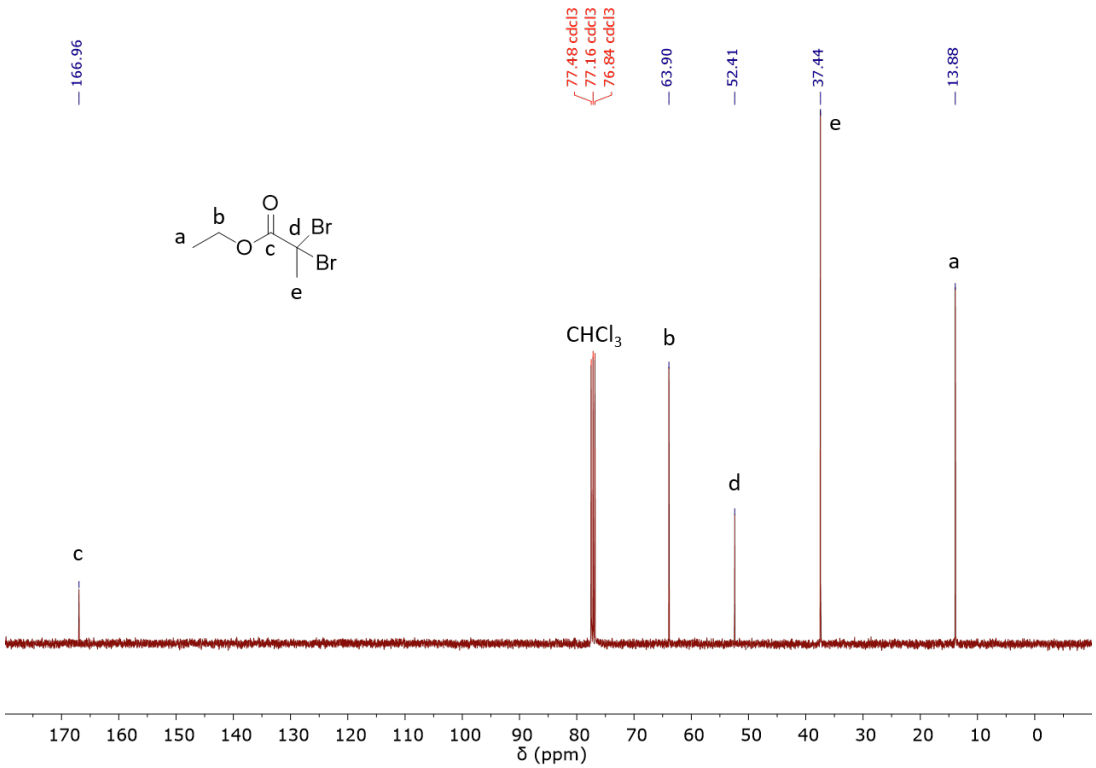

Figure S38. ^{13}C NMR spectrum of EDBP (in $CDCl_3$).

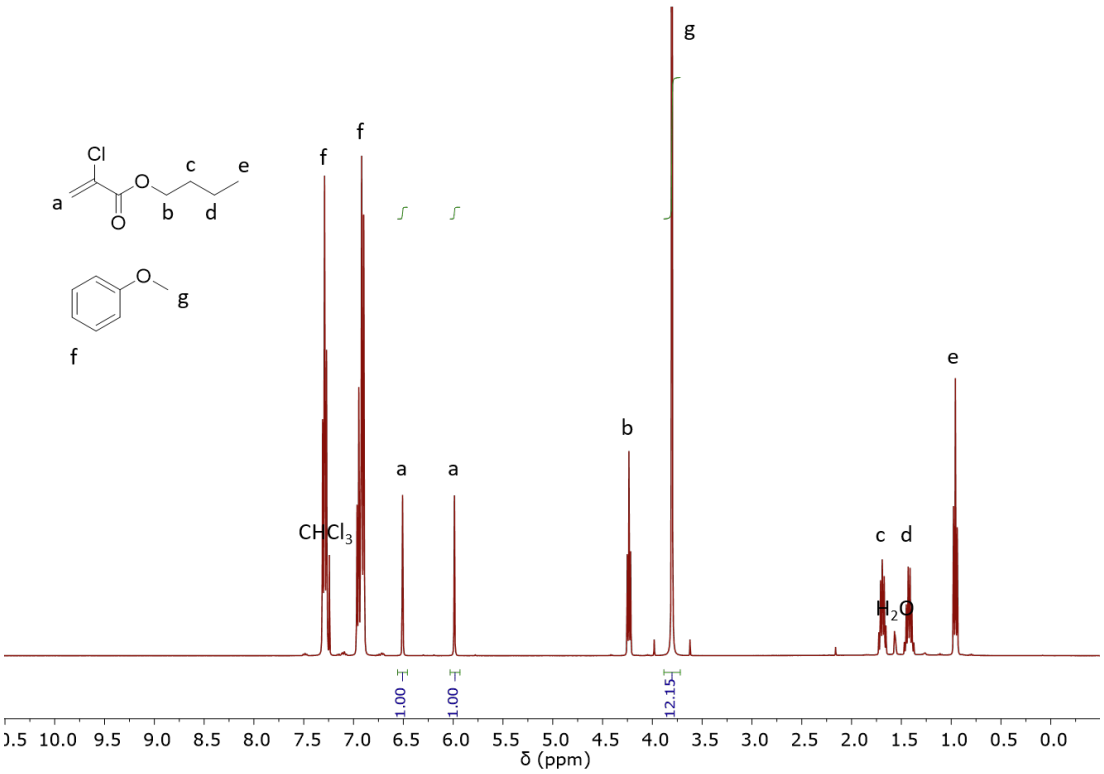

Figure S39. ^{1}H NMR spectrum of BCA in anisole (in $CDCl_3$).

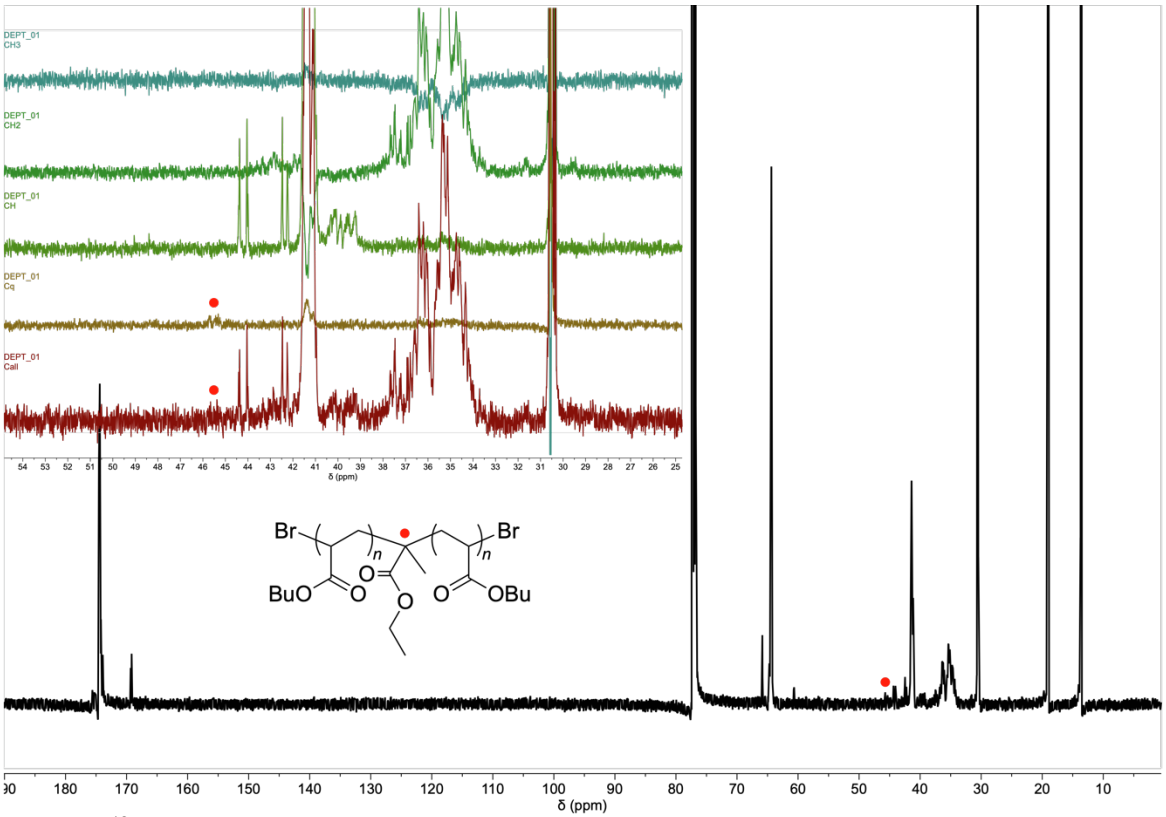

Figure S40. ^{13}C NMR spectrum of linear P*n*BA initiated by EDBP (in $CDCl_3$). Insert: DEPT spectrum.

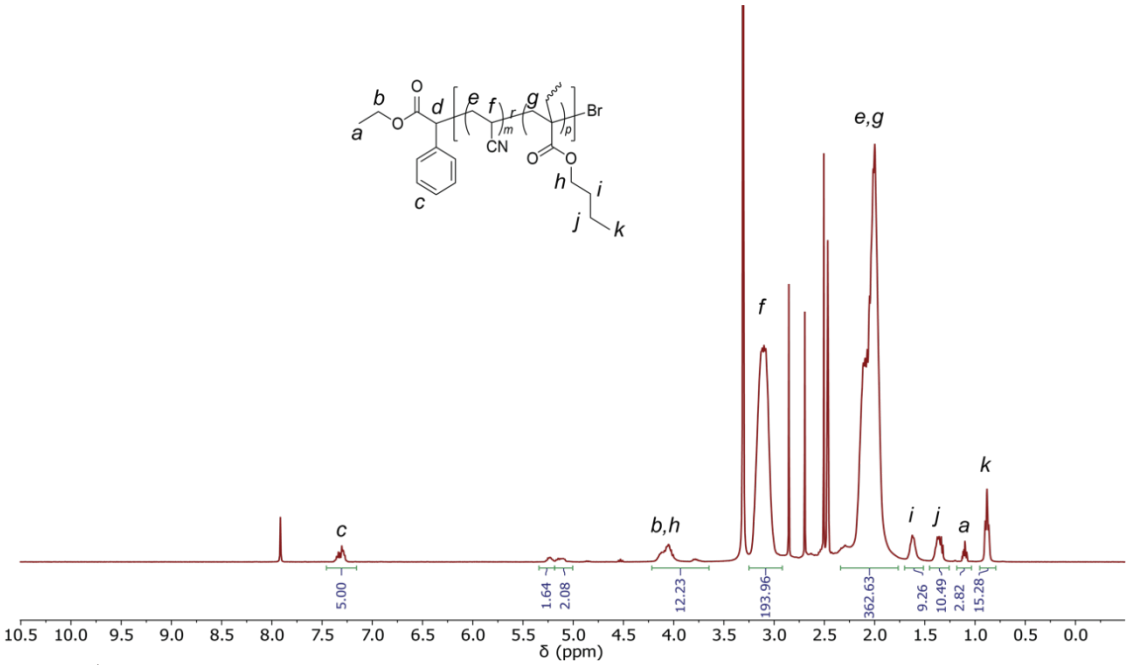

Figure S41. ^{1}H NMR spectrum of branched PAN (Table 1, entry 14) (in DMSO-d_6).

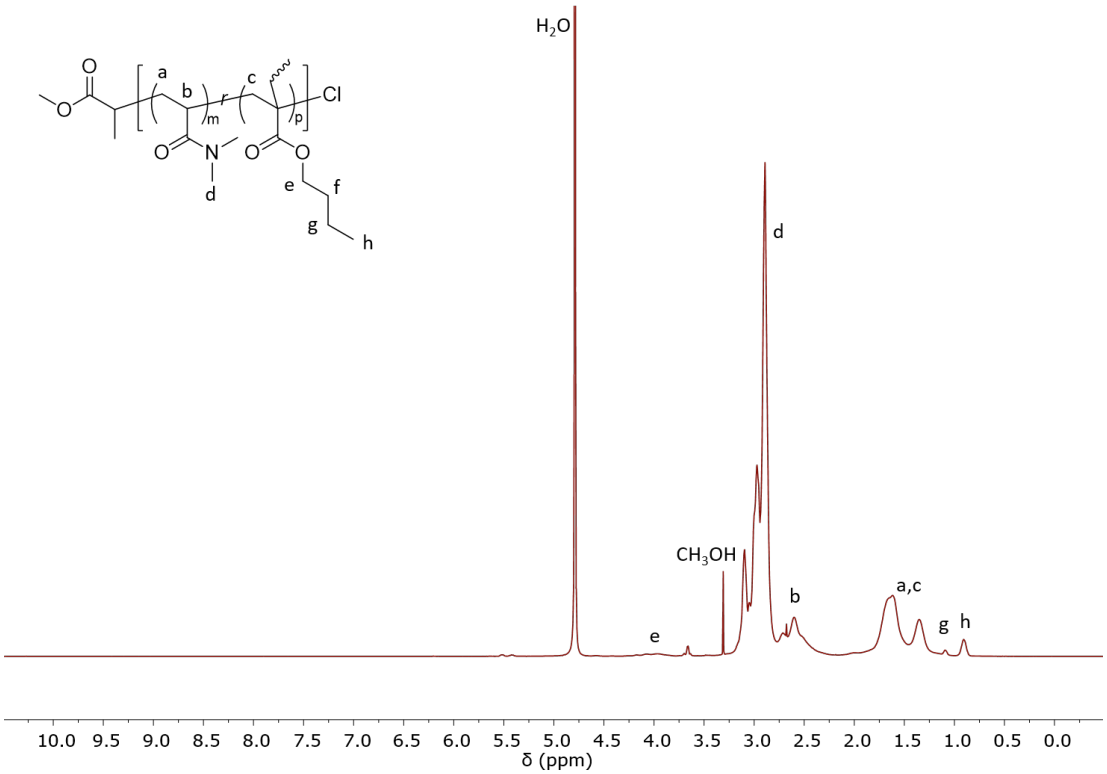

Figure S42. ^{1}H NMR spectrum of branched PDMAA (Table 2, entry 2) (in D_2O).

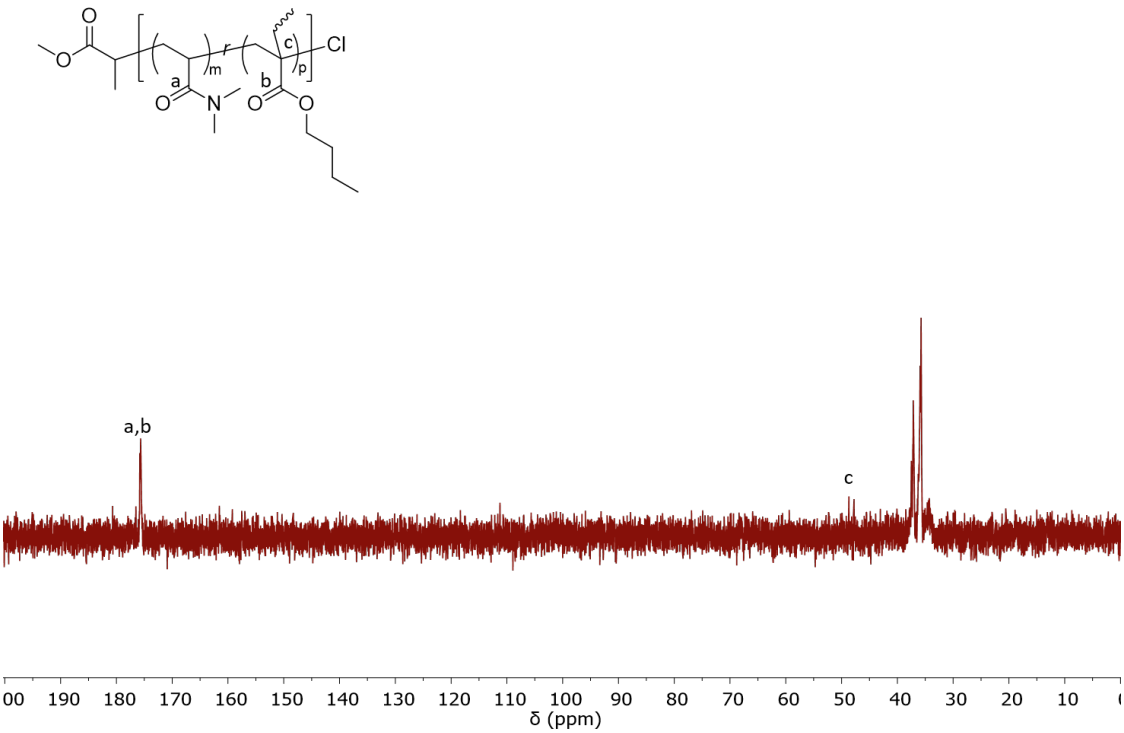

Figure S43. ^{13}C NMR spectrum of branched PDMAA (Table 2, entry 2) (in D_2O).

III. Supplemental References

1. Li, F., Cao, M., Feng, Y., Liang, R., Fu, X., and Zhong, M. (2019). Site-Specifically Initiated Controlled/Living Branching Radical Polymerization: A Synthetic Route toward Hierarchically Branched Architectures. J. Am. Chem. Soc. *141*, 794 – 799. 10.1021/jacs.8b12433.
2. Fang, C., Fantin, M., Pan, X., de Fiebre, K., Coote, M.L., Matyjaszewski, K., and Liu, P. (2019). Mechanistically Guided Predictive Models for Ligand and Initiator Effects in Copper-Catalyzed Atom Transfer Radical Polymerization (Cu-ATRP). J. Am. Chem. Soc. *141*, 7486 – 7497. 10.1021/jacs.9b02158.
3. Braunecker, W.A., Tsarevsky, N.V., Gennaro, A., and Matyjaszewski, K. (2009). Thermodynamic Components of the Atom Transfer Radical Polymerization Equilibrium: Quantifying Solvent Effects. Macromolecules *42*, 6348 – 6360. 10.1021/ma901094s.
4. Fischer, H., and Radom, L. (2001). Factors Controlling the Addition of Carbon-Centered Radicals to Alkenes—An Experimental and Theoretical Perspective. Angew. Chem. Int. Ed. *40*, 1340-1371. 10.1002/1521-3773(20010417)40:8<1340::AID-ANIE1340>3.0.CO;2-#.
5. Knühl, B., Marque, S., and Fischer, H. (2001). Absolute Rate Constants for the Addition of the 1-(tert-Butoxy)carbonylethyl Radical to Alkenes in Solution. Helv. Chim. Acta *84*, 2290-2300. 10.1002/1522-2675(20010815)84:8<2290::AID-HLCA2290>3.0.CO;2-O.
6. Buback, M., Kurz, C.H., and Schmaltz, C. (1998). Pressure dependence of propagation rate coefficients in free-radical homopolymerizations of methyl acrylate and dodecyl acrylate. Macromol. Chem. Phys. *199*, 1721-1727. 10.1002/(SICI)1521-3935(19980801)199:8<1721::AID-MACP1721>3.0.CO;2-5.
7. Tang, W., and Matyjaszewski, K. (2006). Effect of Ligand Structure on Activation Rate Constants in ATRP. Macromolecules *39*, 4953 – 4959. 10.1021/ma0609634.
8. Tang, W., Kwak, Y., Braunecker, W., Tsarevsky, N.V., Coote, M.L., and Matyjaszewski, K. (2008). Understanding Atom Transfer Radical Polymerization: Effect of Ligand and Initiator Structures on the Equilibrium Constants. J. Am. Chem. Soc. *130*, 10702 – 10713. 10.1021/ja802290a.
9. Zhong, M., and Matyjaszewski, K. (2011). How Fast Can a CRP Be Conducted with Preserved Chain End Functionality? Macromolecules *44*, 2668-2677. 10.1021/ma102834s.
10. Buback, M., Egorov, M., Gilbert, R.G., Kaminsky, V., Olaj, O.F., Russell, G.T., Vana, P., and Zifferer, G. (2002). Critically Evaluated Termination Rate Coefficients for Free-Radical Polymerization, 1. The Current Situation. Macromol. Chem. Phys. *203*, 2570 – 2582. 10.1002/macp.200290041.
11. Ballard, N., Salsamendi, M., Santos, J.I., Ruipérez, F., Leiza, J.R., and Asua, J.M. (2014). Experimental Evidence Shedding Light on the Origin of the Reduction of Branching of Acrylates in ATRP. Macromolecules *47*, 964 – 972. 10.1021/ma4025637.
12. Seeliger, F., and Matyjaszewski, K. (2009). Temperature Effect on Activation Rate Constants in ATRP: New Mechanistic Insights into the Activation Process. Macromolecules *42*, 6050 – 6055. 10.1021/ma9010507.
13. Fischer, H., and Paul, H. (1987). Rate constants for some prototype radical reactions in liquids by kinetic electron spin resonance. Acc. Chem. Res. *20*, 200 – 206. 10.1021/ar00137a007.